Applied Physics Reviews

Hopf bifurcations in electrochemical, neuronal, and semiconductor systems analysis by impedance spectroscopy

Cite as: Appl. Phys. Rev. **9**, 011318 (2022); https://doi.org/10.1063/5.0085920
Submitted: 20 January 2022 • Accepted: 28 February 2022 • Published Online: 16 March 2022

Juan Bisquert

Applied Physics Reviews REVIEW scitation.org/journal/are

Hopf bifurcations in electrochemical, neuronal, and semiconductor systems analysis by impedance spectroscopy

Cite as: Appl. Phys. Rev. 9, 011318 (2022); doi: 10.1063/5.0085920
Submitted: 20 January 2022 · Accepted: 28 February 2022 ·
Published Online: 16 March 2022

View Online Export Citation CrossMark

Juan Bisquert[1,2,a)]

AFFILIATIONS

[1]Institute of Advanced Materials (INAM), Universitat Jaume I, 12006 Castelló, Spain
[2]Yonsei Frontier Lab, Yonsei University, Seoul 03722, South Korea

[a)]Author to whom correspondence should be addressed: bisquert@uji.es

ABSTRACT

Spontaneous oscillations in a variety of systems, including neurons, electrochemical, and semiconductor devices, occur as a consequence of Hopf bifurcation in which the system makes a sudden transition to an unstable dynamical state by the smooth change of a parameter. We review the linear stability analysis of oscillatory systems that operate by current–voltage control using the method of impedance spectroscopy. Based on a general minimal model that contains a fast-destabilizing variable and a slow stabilizing variable, a set of characteristic frequencies that determine the shape of the spectra and the associated dynamical regimes are derived. We apply this method to several self-sustained rhythmic oscillations in the FitzHugh–Nagumo neuron, the Koper–Sluyters electrocatalytic system, and potentiostatic oscillations of a semiconductor device. There is a deep and physically grounded analogy between different oscillating systems: neurons, electrochemical, and semiconductor devices, as they are controlled by similar fundamental processes unified in the equivalent circuit representation. The unique impedance spectroscopic criteria for widely different variables and materials across several fields provide insight into the dynamical properties and enable the investigation of new systems such as artificial neurons for neuromorphic computation.

TABLE OF CONTENTS

I. INTRODUCTION

Bifurcation is an abrupt qualitative change of the behavior of a dynamical system by the smooth variation of a control parameter. Hopf bifurcation[1–5] causes the emergence of self-sustained oscillation from a stable fixed point. Although bifurcations happen in highly nonlinear systems with large amplitude oscillations in unstable domains, the linearized equations around a given stationary point contain significant information about the evolution of the system. The dynamical regimes are classified by normal mode method analysis.[6] In systems that operate electrically or electrochemically, the linearized current–voltage perturbation at different measuring angular frequencies ω produces the method of impedance spectroscopy (IS). This technique is widely used in electrochemistry and materials science for the analysis of physico-chemical processes and the characterization of dynamical behavior.[7–9] The impedance spectra are measured at different steady states, and are what allows us to formulate an equivalent circuit (EC) model in which the circuit elements depend on the external parameter as the voltage or current. The EC technique provides an excellent approach to summarize the measured spectral shapes and obtain an interpretation of the internal mechanisms and dynamical evolution of the system. In this paper, we show a unified analysis of systems that have in common transition from rest to spiking state by Hopf bifurcations using the method of small signal IS.

The analysis of oscillating systems using IS criteria has been amply exploited in the field of electrochemical oscillators caused by catalytic, electrodeposition, and electrodissolution reactions in metal[10–12] and semiconductor[13,14] electrodes. In particular, the Hopf bifurcation has been described by means of electrochemical impedance spectroscopy.[15–18]

Excitability of neurons is determined by Hopf bifurcation in which the neuron starts to repetitively fire an action potential under certain stimulus. For more than one century, the neuronal activity has been analyzed by the methods of electrical circuits[19–21] and the impedance measurements were important to derive the paradigm of membrane excitability by Hodgkin and Huxley (HH)[21] that underpins the current understanding of neuronal activity.[22] The development of neuromorphic systems that use physical artificial neurons to do computations holds promise for building artificial intelligence closely coupled to perceptual systems.[23–26] Memristor devices can produce compact and reliable artificial neurons and synapses for computation algorithms based on neuron spiking.[27–33] Recently, some equivalent circuits using inductors and memristors have been used for simulation of repetitive neuron firing.[34–37]

In summary, bifurcations controlled by an external voltage u and current I_{tot} are found in electrochemistry,[10] neuroscience,[38,39] and semiconductor devices,[40] but a unified analysis of insight obtained in different fields is not complete. We present a general characterization of the dynamics of two variable systems that show self-sustained oscillations using IS. Since electrochemical and semiconductor processes exponentially depend on the applied voltage, a rapid succession of very different impedance spectra due to the changes of dynamical regimes and bifurcations has been often reported.[14,41] Our aim is to provide an integrated view of different impedance spectra based on EC methods that enable to recognize the underlying model starting from experimental measurements of IS. We show that the bifurcation and dynamical properties can be directly obtained from conditions of the EC elements.[30]

As an introduction, we revise in Sec. II the well-known stability and linear response properties of a general minimal two-dimensional non-linear system. Next, in Sec. III, we formulate the dynamical properties in terms of impedance criteria, introducing a set of characteristic frequencies that completely characterize the impedance and dynamical properties. In Sec. IV, we illustrate with several examples the application of the IS characterization for systems that show rhythmic oscillations at fixed current. In Sec. V, we show the analysis of oscillation at fixed voltage. In Sec. VI, we end with some conclusions.

II. Hopf BIFURCATION IN A TWO-DIMENSIONAL DYNAMICAL SYSTEM

A. The model

The description of Hopf bifurcation requires separation of a fast destabilizing variable (u) and a slow stabilizing variable (x).[17] The simplest approach to bifurcation in nonlinear systems consists, therefore, of two-dimensional models. Models that use the essential oscillating variables play a central role in neuroscience and in electrochemical oscillators.[38,42] When the nonlinear system of differential equations undergoes Hopf bifurcation, there arises a limit cycle, that is, a closed and isolated trajectory in the phase portrait $u \times x$.

Consider the voltage u and current I_{tot} and an additional internal state variable x. The dynamical model is defined by the following equations:

$$\tau_u \frac{du}{dt} = f(u, x, I_{tot}), \tag{1}$$

$$\tau_k \frac{dx}{dt} = g(u, x). \tag{2}$$

τ_u, τ_k are the characteristic times of the fast variable u and the slow variable x, respectively, and we have $\tau_u \ll \tau_k$, although the opposite condition is formally possible.

The functions f and g are, in general, nonlinear functions that define the properties of the model. As an example, we show the FitzHugh–Nagumo (FHN) neuron equations,[34]

$$f = -\frac{u^3}{3} + u - R_I x + R_I I_{tot}, \tag{3}$$

$$g = \frac{1}{R_w} u - bx. \tag{4}$$

The FHN model has been broadly studied by its rich phase portraits.[38,43–45] The physical variables are the membrane voltage u, the transmembrane current I_{tot}, and an internal recovery current x, which represents the changes in ion-channel conductance as a function of the voltage. The model introduces a set of specific parameters that establish possible bifurcations and qualitatively different dynamical evolutions: the voltage response time τ_u, the recovery current response time τ_x, a channel resistor R_I, a recovery current resistor R_w, and a modulation constant b. All these numbers are positive. The dynamical response is shown in Fig. 1. It is determined by the numbers indicated in the figure caption: the set of FHN model parameters, the specific voltage associated with the fixed current, the equivalent circuit elements, and the characteristic frequencies as discussed later.

Equations (1) and (2) are not symmetrical, as the external current I_{tot} appears only in the equation of the first variable. Equation (2), that describes the slowing down kinetics, establishes a voltage-controlled system as in the usual neuron models.[21,38] It is otherwise possible to establish current-controlled systems by introducing $h(I_{tot}, x)$ in Eq. (2).[46,47]

Consider the steady state situation in which the time derivatives are zero. The phase portrait of the system (1) and (2) is controlled by the nullclines,

$$f(u, x, I_{tot}) = 0, \tag{5}$$

$$g(u, x) = 0. \tag{6}$$

An equilibrium point is the solution of Eqs. (5) and (6). It is determined by the intersection of the nullcline curves, as shown in Fig. 1(c). At any fixed point, we have a solution of Eq. (6),

$$x = x(u). \tag{7}$$

Hence, introducing Eq. (7) in (5), we obtain the equilibrium value,

$$I_{tot} = I_{tot}(u). \tag{8}$$

This is the current–voltage curve of the system shown in Fig. 1(a) for the FHN model. It is useful to plot the vector field $\{\dot{u}, \dot{x}\}$ by the representation of $\{f/\tau_u, g/\tau_k\}$. The field lines indicate the possible trajectories, and the nullclines are the points of zero velocity, Figs. 1(c)

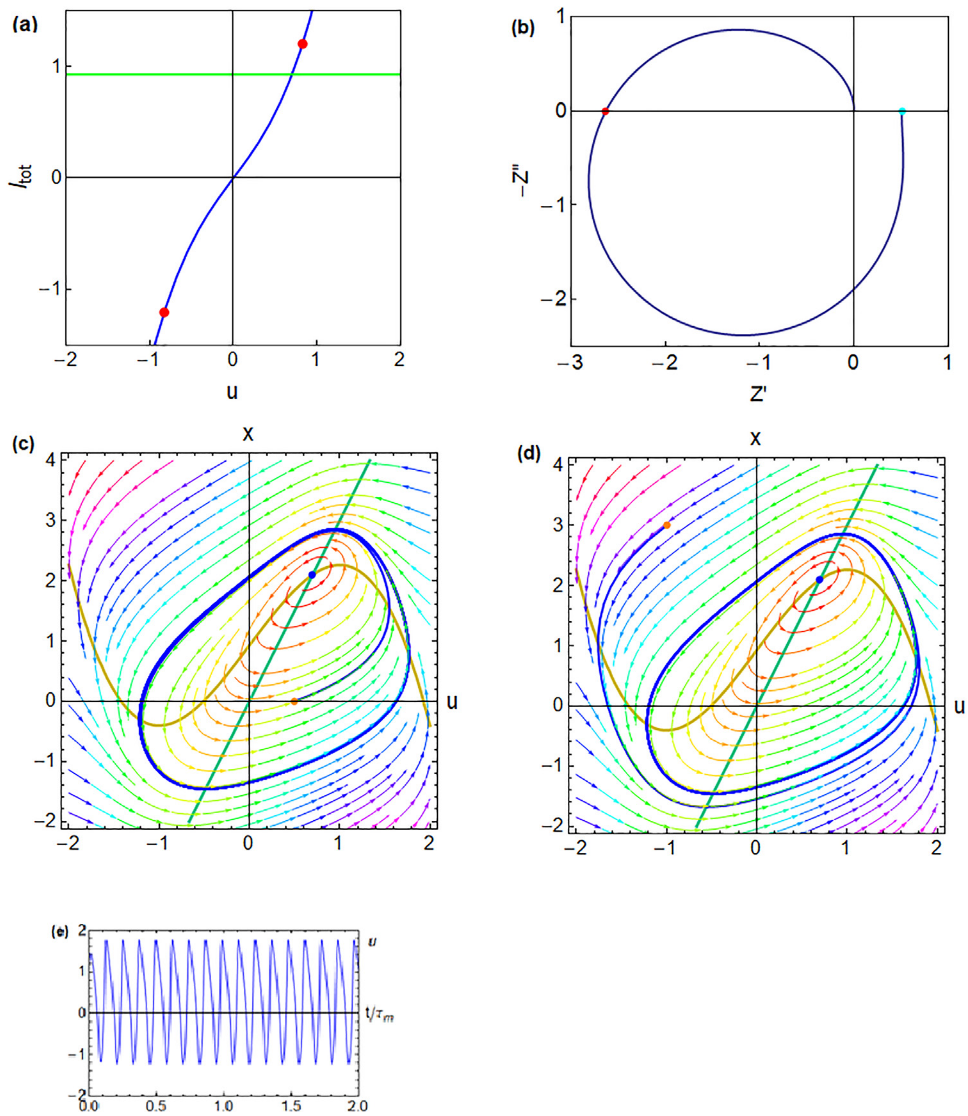

FIG. 1. Dynamical properties in a realization of the FHN model. (a) Current–voltage curve. The green line is the current obtained at $u = 0.7$. The red points are Hopf bifurcations. (b) Impedance spectrum, indicating the characteristic frequencies $\omega = 0$ (cyan) and the crossing of the horizontal axis (red, ω_c). (c) Nullclines, trajectories, and vector velocities. The *f*-nullcline is the yellow line, and *g*-nullcline is the green line. The blue point is the fixed point at the nominal potential. The orange point is the starting condition. Color streamlines indicate the norm of the vector field. (d) Trajectories at a different starting condition. (e) Voltage evolution with time. Parameters: $R_l = 0.5$, $b = 0.8$, $r = 1.2$, $\epsilon = 0.4$, $\tau_m = 0.01$, $u = 0.7$, $\{R_a, R_b, L_a, C_m\} = \{0.333, -0.980, 0.0104, 0.02\}$, and $\{\omega_a, \omega_b, \omega_L, \omega_c, \omega_o, R_{dc}, -\omega_L - \omega_b\} = \{150, -51, 32, 61.5, 56.3, 0.505, 19\}$.

and 1(d). We fix a value of the external current, as shown by the green line in Fig. 1(a), and we solve Eqs. (3) and (4) starting from a point out of equilibrium (orange in the phase portrait plot) that represents a perturbation of the system. In Figs. 1(c) and 1(d), we observe that the trajectories, starting from any point in the plane, lead to a periodic stable trajectory in the phase plane that never passes through the equilibrium point, a limit cycle. The observable oscillations of the voltage are shown in Fig. 1(e). We present in Fig. 1(b) the impedance spectrum associated with the given point. We aim to show how to extract important information from the spectral shape.

B. Dynamical stability

When we change the fixed current in Fig. 1, we move the f-nullcline and generate different fixed point. To analyze the dynamics at a given point, we consider a linear stability analysis of Eqs. (1) and (2). The linearized equations are

$$\tau_u \frac{d\hat{u}}{\mathrm{dt}} = f_u \hat{u} + f_x \hat{x} + f_I \hat{I}_{tot}, \quad (9)$$

$$\tau_x \frac{d\hat{x}}{\mathrm{dt}} = g_u \hat{u} + g_x \hat{x}. \quad (10)$$

The Jacobian is

$$\begin{pmatrix} \dfrac{f_u}{\tau_u} & \dfrac{f_x}{\tau_u} \\ \dfrac{g_u}{\tau_x} & \dfrac{g_x}{\tau_x} \end{pmatrix}. \quad (11)$$

The eigenvalues λ are determined by the following equation:

$$\lambda^2 - T_\lambda \lambda + \Delta = 0, \quad (12)$$

where T_λ is the trace and Δ is the determinant of the Jacobian, which expressions are given in Table I. The roots are

$$\lambda_{1,2} = \frac{1}{2}\left(T_\lambda \pm \sqrt{D_\lambda}\right), \quad (13)$$

where the discriminant is

TABLE I. Parallel circuit: Model parameters and derived quantities.

Parameters/variables	Code	Equivalent circuit	General dynamical model	FitzHugh–Nagumo	Koper–Sluyters
			τ_u	τ_m	ε
			τ_x	τ_x	1
			R_I	R_I	1
Specific parameters				$b, R_w, \varepsilon = \dfrac{\tau_m}{\tau_x}, r = \dfrac{R_I}{R_w}$	$k_a(u),\ k_e(u)$
C_m			$\dfrac{\tau_u}{R_I}$	$\dfrac{\tau_m}{R_I}$	ε
R_a			$\dfrac{R_I g_x}{f_x g_u}$	bR_w	$\dfrac{1}{k_e}\dfrac{(k_a+k_e)^2}{k_e k_a' - k_a k_e'}$
R_b			$-\dfrac{R_I}{f_u}$	$(u^2-1)^{-1}R_I$	$\dfrac{k_a+k_e}{k_a k_e'}$
L_a			$-\dfrac{R_I \tau_x}{f_x g_u}$	$\tau_x R_w$	$\dfrac{1}{k_e}\dfrac{k_a+k_e}{k_a' k_e - k_a k_e'}$
$\dfrac{R_a}{L_a}$			$-\dfrac{g_x}{\tau_x}$	$\dfrac{b}{\tau_x}$	k_a+k_e
R_{dc}		$\left(\dfrac{1}{R_a}+\dfrac{1}{R_b}\right)^{-1}$	$-\dfrac{R_I g_x}{\tau_u \tau_x \Delta}$	$R_I\left[u^2-1+\dfrac{r}{b}\right]^{-1}$	$\dfrac{(k_a+k_e)^2}{k_e^2 k_a' + k_a^2 k_e'}$
ω_a		$\dfrac{1}{R_a C_m}$		$\dfrac{r}{b\tau_u}$	$\dfrac{k_e}{\varepsilon}\dfrac{k_e k_a' - k_a k_e'}{(k_a+k_e)^2}$
ω_b		$\dfrac{1}{R_b C_m}$	$-\dfrac{f_u}{\tau_u}$	$\dfrac{1}{\tau_m}(u^2-1)$	$\dfrac{1}{\varepsilon}\dfrac{k_a k_e'}{k_a+k_e}$
$-\omega_b$					
ω_L		$\dfrac{R_a}{L_a}$	$-\dfrac{g_x}{\tau_x}$	$\dfrac{b\varepsilon}{\tau_u}$	k_a+k_e
ω_c		$[\omega_L(\omega_a-\omega_L)]^{1/2}$		$\dfrac{b}{\tau_m}\left[\varepsilon\left(\dfrac{r}{b^2}-\varepsilon\right)\right]^{1/2}$	
Z_1'		$\dfrac{R_b}{1+\dfrac{R_a R_b C_m}{L_a}}$			
ω_d		$\omega_L\left(-\dfrac{\omega_a}{\omega_b}-1\right)^{1/2}$		$\dfrac{b\epsilon}{\tau_m}\left(\dfrac{r}{b}\dfrac{1}{1-u^2}-1\right)^{1/2}$	
Δ		$\omega_L(\omega_a+\omega_b)$	$\dfrac{1}{\tau_u\tau_x}(f_u g_x - f_x g_u)$	$\dfrac{b\varepsilon}{\tau_m^2}\dfrac{R_I}{R_{dc}} = \dfrac{\varepsilon}{\tau_m^2}[b(u^2-1)+r]$	$\dfrac{1}{\varepsilon}\dfrac{k_a+k_e}{R_{dc}} = \dfrac{1}{\varepsilon}\dfrac{k_e^2 k_a' + k_a^2 k_e'}{k_a+k_e}$
ω_o		$[\omega_L(\omega_a+\omega_b)]^{1/2}$	$\Delta^{1/2}$	$\dfrac{1}{(\tau_m\tau_x)^{1/2}}[b(u^2-1)+r]^{1/2}$	$\left(\dfrac{1}{\varepsilon}\dfrac{k_e^2 k_a' + k_a^2 k_e'}{k_a+k_e}\right)^{1/2}$
T_λ		$-\omega_b-\omega_L$	$\dfrac{f_u}{\tau_u}+\dfrac{g_x}{\tau_x}$	$\dfrac{1}{\tau_m}(1-u^2-b\varepsilon)$	$-\left(k_a+k_e+\dfrac{1}{\varepsilon}\dfrac{k_a k_e'}{k_a+k_e}\right)$
$u_{Hopf}\ (\omega_L = -\omega_b)$		$\dfrac{R_a R_b C_m}{L_a} = -1$		$\pm(1-b\varepsilon)^{1/2}$	$k_e' = -\varepsilon\dfrac{(k_a+k_e)^2}{k_a}$

$$D_\lambda = T_\lambda^2 - 4\Delta. \quad (14)$$

The Hopf bifurcation occurs when a pair of eigenvalues become purely imaginary, i.e., the real part of the eigenvalue changes sign from negative to positive.[4,5] It happens for $\Delta > 0$ when $\mathrm{Re}(\lambda) = 0$ and $\mathrm{Im}(\lambda) \neq 0$. We write $\lambda = i\omega_o$ and we obtain from (12),

$$-\omega_o^2 - iT_\lambda\omega_o + \Delta = 0. \quad (15)$$

$T_\lambda = 0$ is the Hopf bifurcation, and the oscillation frequency is $\omega_o = \Delta^{1/2}$.

For $\Delta > 0$ and $T_\lambda > 0$, the fixed point becomes an unstable source and generates a limit cycle trajectory. In the region $T_\lambda > 0$, $D_\lambda > 0$, the eigenvalues are real and positive indicating an unstable node. For $T_\lambda > 0$, $D_\lambda < 0$ the eigenvalues are complex-conjugate in an unstable focus in which the trajectories spiral away from the fixed point. $\Delta < 0$ indicates an unstable saddle region with real eigenvalues of different signs. A complete classification of equilibria and the local stability properties are explained in many excellent books.[3,6,38] Plotting the different quantities T_λ, Δ and D_λ, we can observe the nature of the fixed point. In Fig. 2, we show different dynamic regimes of the FHN model for two sets of parameters and the corresponding stability graphs.

In Figs. 2(a)–2(c), the current–voltage is monotonic as Δ is always positive. The stability plot in Fig. 2(c) indicates two different regimes. For $T_\lambda < 0$, the fixed point is stable, and the trajectory leads to this equilibrium point as shown in Fig. 3. In the region $T_\lambda > 0$, the fixed point is unstable as shown in Fig. 1. The trajectories lead to a stable limit cycle, which spins around the fixed point, either starting inside of the cycle, Fig. 1(c), or from outside in Fig. 1(d). This is the domain of sustained oscillations of the voltage as indicated in Fig. 1(e) as in a spiking neuron.

In Figs. 2(b)–2(d), the parameters lead to an unstable region of observable negative resistance in which $\Delta < 0$. The experiment can be performed by fixing either the current (galvanostatic mode in electrochemistry) or the voltage (potentiostatic mode), When the current has a N-shape as in Fig. 2(b), the voltage is single-valued but a fixed current provides three different fixed points, a saddle, and two sinks. If the current has an S-shape, the opposite situation happens, and the curve will be single valued for a fixed current. In Fig. 2(b), fixed current allows three fixed points. One example is shown in Fig. 4. The central point is unstable, and the trajectories can lead to either A or C, depending on the initial conditions, as shown by the flux lines. These features are further discussed in Sec. IV A.

When we trace the current–voltage curve by changing the fixed current parameter, the dynamical properties are reflected in qualitatively different measurable impedance spectra as shown in Figs. 1, 3, and 4. The evolution of the spectra for an electrochemical model by Koper and Sluyters (KS) is shown in Fig. 5 from their pioneering

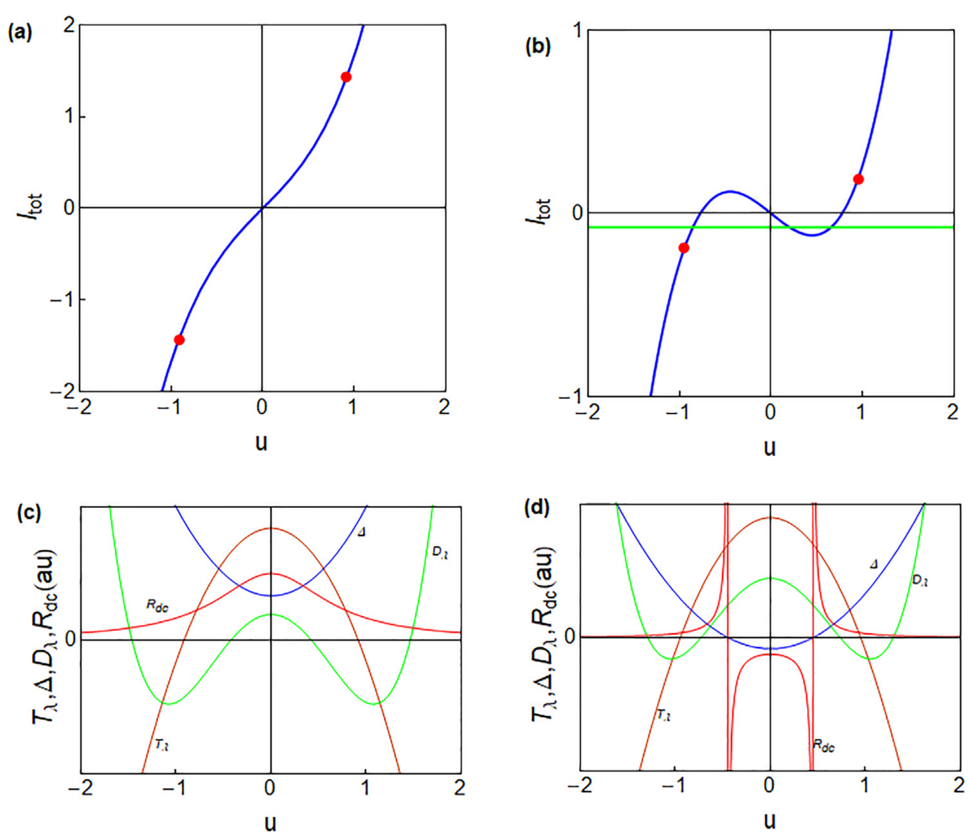

FIG. 2. Two different realizations of the FHN model, indicating the current–voltage curves [(a) and (b)] and the stability parameters [(c) and (d)]. [(a)–(c)] $b = 0.8$, $r = 1.2$, $\epsilon = 0.2$, and $\tau_m = 0.01$; [(b)–(d)] $b = 1$, $r = 0.8$, $\epsilon = 0.1$, and $\tau_m = 0.01$.

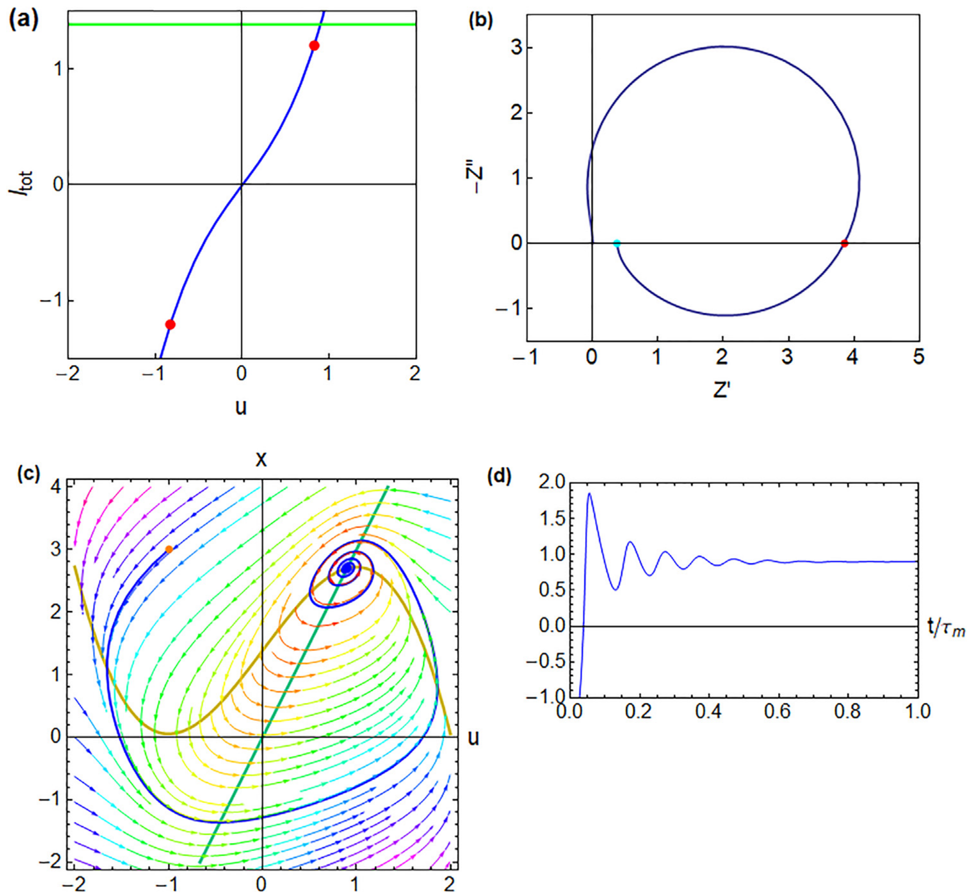

FIG. 3. Dynamical properties in a realization of the FHN model. (a) Current–voltage curve. The green line is the current obtained at $u = 0.9$. The red points are the Hopf bifurcations. (b) Impedance spectrum, indicating the characteristic frequencies $\omega = 0$ (cyan) and the crossing of the horizontal axis (red, ω_c). (c) Nullclines, trajectories, and vector velocities. The f-nullcline is the yellow line, and the g-nullcline is the green line. The orange point is the starting condition. (d) Voltage evolution with time. Parameters: $R_I = 0.5$, $b = 0.8$, $r = 1.2$, $\epsilon = 0.4$, $\tau_m = 0.01$, $u = 0.9$, $\{R_a, R_b, L_a, C_m\} = \{0.333, -2.63, 0.0104, 0.02\}$, and $\{\omega_a, \omega_b, \omega_L, \omega_c, \omega_o, R_{dc}, -\omega_L - \omega_b\} = \{150, -19, 32, 61.4, 64.7, 0.382, -13\}$.

papers[48,49] and discussed later in Sec. IV B. Our objective in Secs. III A–III C is to establish a general classification of the conditions that generate different spectra and the related dynamics.

III. GENERAL EQUIVALENT CIRCUIT OF A TWO-DIMENSIONAL SYSTEM

A. Impedance parameters

To calculate the ac impedance of the general model, we take the Laplace transform of the small perturbation Eqs. (9) and (10), $d/dt \rightarrow s$, where $s = i\omega$. The following resistance will be considered constant:

$$R_I = f_I. \tag{16}$$

We obtain

$$Z(s)^{-1} = \frac{\hat{I}_{tot}}{\hat{u}} = \frac{1}{R_I}\left(s\tau_u - f_u - \frac{f_x g_u}{s\tau_x - g_x}\right). \tag{17}$$

We can write the impedance function in terms of equivalent circuit elements defined in the fourth column of Table I,

$$Z(s) = \left[C_m s + R_b^{-1} + (R_a + L_a s)^{-1}\right]^{-1}. \tag{18}$$

This model corresponds to the equivalent circuit presented in Fig. 6. The EC is highly characteristic for memristors,[30,50] oscillating neurons,[34] and electrocatalytic models.[51] In this paper, the capacitor C_m is considered a passive charging element, such as a double layer or depletion region, and it is taken strictly positive. The inductor L_a and the resistors R_a, R_b can be either positive or negative. The inductor that arises from Eqs. (1) and (2) in Fig. 6 for neuronal and electrochemical systems does not have the usual interpretation from electromagnetism as a coiled wire. Instead it has been denominated a "chemical inductor," see Ref. 37 for a discussion of this point.

We remark that the ECs of impedance models can be expressed in several equivalent formulation due to the possibility of internal

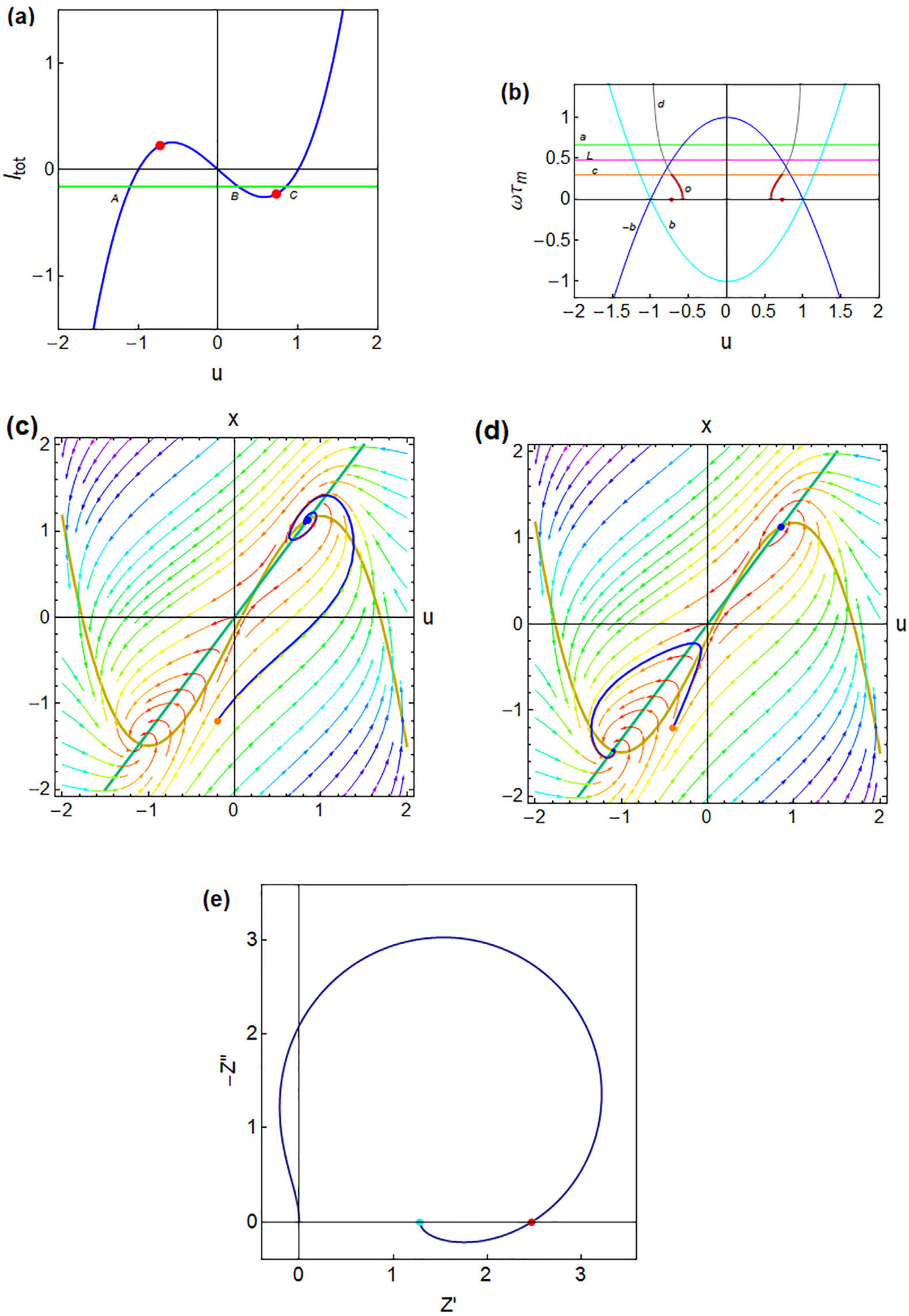

FIG. 4. A FHN model behavior for a potential in point C of the $I-u$ curve (a). The red points are Hopf bifurcations. (b) Map of characteristic frequencies. [(c) and (d)] Nullclines, trajectories, and vector velocities. The *f*-nullcline is the yellow line, and the *g*-nullcline is the green line. The orange point is the starting condition. The blue point is the fixed point at the nominal potential. (e) Impedance spectrum, indicating the characteristic frequencies $\omega = 0$ (cyan) and the crossing of the horizontal axis (red, ω_c). Parameters: $R_l = 0.5$, $b = 1.2$, $r = 0.8$, $\epsilon = 0.4$, $\tau_m = 0.01$, $u = 0.85$ (point C), $\{R_a, R_b, L_a, C_m\} = \{0.75, -1.80, 0.0156, 0.02\}$, and $\{\omega_a, \omega_b, \omega_L, \omega_c, \omega_o, R_{dc}, -\omega_L -\omega_b\} = \{66.7, -27.7, 48., 29.9, 43.2, 1.28, -20.2\}$.

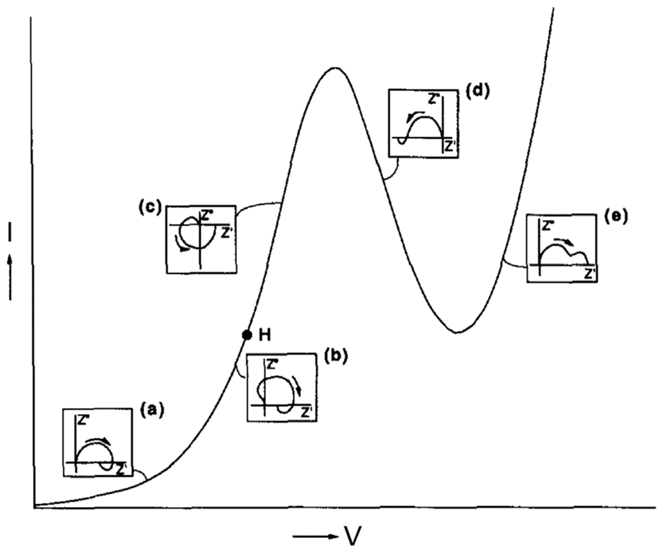

FIG. 5. Qualitatively different impedance plots obtained at different parts of the current–voltage curve in the Koper–Sluyters model. The arrows indicate the direction of decreasing frequency, and H indicates the current value for which Hopf bifurcation is observed under galvanostatic conditions. Reproduced with permission from Koper and Sluyters, J. Electroanal. Chem. **149**, 371 (1994). Copyright 1994 Elsevier.[48]

linear transformations.[52,53] However, we use here the circuit in Fig. 6 that has the most direct physical interpretation. The negative capacitance feature[8] arises from the inductor element.

B. Classification of impedance spectra

The impedance function (18) associated with the EC of Fig. 6 can be written in terms of certain characteristic frequencies,

$$Z(s) = \frac{R_I}{\tau_u}\left[s + \omega_b + \frac{\omega_a}{\left(1 + \frac{s}{\omega_L}\right)}\right]^{-1}. \tag{19}$$

The frequencies are

$$\omega_a = \frac{1}{R_a C_m}, \tag{20}$$

$$\omega_b = \frac{1}{R_b C_m}, \tag{21}$$

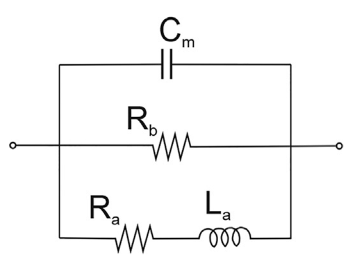

FIG. 6. Equivalent circuit of the two-dimensional general dynamical model.

$$\omega_L = \frac{R_a}{L_a}. \tag{22}$$

In Eq. (19), R_I establishes the scale of the impedance, and τ_u sets the rescaling of the frequency/time. Below we plot the characteristic frequencies in the dimensionless form $\omega_i \tau_u$. Using different combinations of the characteristic frequencies, a variety of qualitatively different spectra can be generated as shown in Fig. 7.

The dc resistance

$$Z(\omega = 0) = R_{dc} \tag{23}$$

has the value

$$R_{dc}^{-1} = C_m(\omega_a + \omega_b) = \frac{1}{R_a} + \frac{1}{R_b} = -\frac{R_I g_x}{\tau_u \tau_x \Delta}. \tag{24}$$

According to the last equality, shown in Table I, the dc resistance and the determinant Δ have the same sign if

$$g_x < 0. \tag{25}$$

As an example, this is satisfied in Eq. (4). Equation (25) is the condition that x is the stabilizing variable, and we require that it is satisfied. Hence, the sign of the dc resistance is a faithful representation of the stability condition $\Delta > 0$.

We establish the properties of the impedance spectra by calculating the points of intercept with the axis. The equation

$$Z''(\omega) = 0 \tag{26}$$

that sets the imaginary part of the impedance Z'' to zero has a solution at $\omega = 0$. However, there can exist another crossing given by the condition

$$Z_1' = R_{Z''=0} = \frac{R_b}{1 + \frac{R_a R_b C_m}{L_a}}. \tag{27}$$

If we calculate the frequency of intercept in Eq. (27), we obtain

$$\omega_c = [\omega_L(\omega_a - \omega_L)]^{1/2}. \tag{28}$$

The hook in Fig. 7(b) is observed when ω_c is real. If $\omega_L > 0$, then Fig. 7(b) is obtained when

$$\omega_a > \omega_L. \tag{29}$$

The condition of intercept with the vertical axis is

$$Z'(\omega) = 0. \tag{30}$$

The resulting frequency is

$$\omega_d = \omega_L\left(-\frac{\omega_a}{\omega_b} - 1\right)^{1/2}. \tag{31}$$

When there is interception of the vertical axis, ω_d is real, as in Figs. 7(c)–7(m). If ω_a, $\omega_L > 0$, then ω_d can be real only with negative resistance R_b that causes $\omega_b < 0$.

All the spectra in Fig. 7 correspond to distinct combinations of the characteristic frequencies. Only the pairs k, m, and n, p, are qualitatively the same behavior, corresponding to both negative R_a, L_a. This situation is termed "edge of chaos" in the work of Chua.[46,54,55]

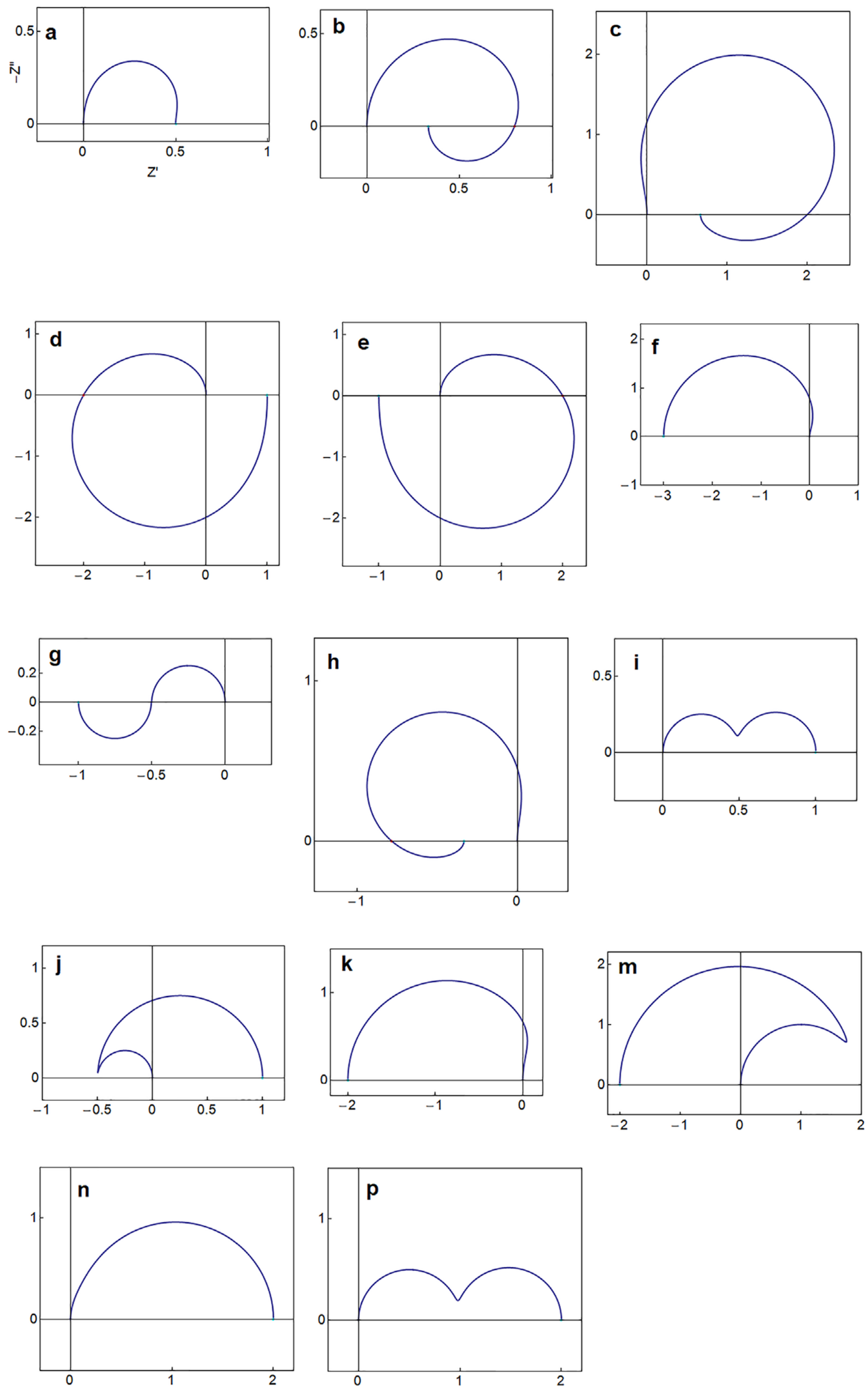

FIG. 7. Complex plane impedance representation of the spectral patterns of the parallel impedance model in Fig. 6. Parameters $\{R_a, R_b, L_a, C_m\}$ $\{\omega_a, \omega_b, \omega_L, \omega_c, \omega_d, \omega_o, R_{dc}, -\omega_L - \omega_b\}$. (a) $\{1, 1, 0.5, 1\}$ $\{1, 1, 2, \mathrm{Im}, \mathrm{Im}, 2, \frac{1}{2}, -3\}$, (b) $\{\frac{1}{2}, 1, 2, 1\}$ $\{2, 1, \frac{1}{4}, 0.657, \mathrm{Im}, 0.866, \frac{1}{3}, -\frac{5}{4}\}$, (c) $\{1, -2, 0.5, 1\}$ $\{2, -\frac{1}{2}, 1, 1, 1.73, 1.22, \frac{2}{3}, -0.5\}$, (d) $\{\frac{1}{2}, -1, 1, 1\}\{2, -1, \frac{1}{2}, 0.866, 0.5, 0.707, 1, \frac{1}{2}\}$, (e) $\{-\frac{1}{2}, 1, 1, 1\}$ $\{-2, 1, -\frac{1}{2}, 0.866, -0.5, 0.707, -1, -\frac{1}{2}\}$, (f) $\{-\frac{1}{2}, 0.6, 0.11, 1\}\{-2, 1.67, -4.54, \mathrm{Im}, -2.03, 1.23, -3.00, 2.88\}$, (g) $\{1, -\frac{1}{2}, 100, 1\}$ $\{1, -2, 0.01, 0.0995, \mathrm{Im}, \mathrm{Im}, -1, 1.99\}$, (h) $\{-\frac{1}{4}, 1, 0.11, 1\}\{-4, 1, -2.27, 1.98, -3.93, 2.62, -\frac{1}{3}, 1.27\}$, (i) $\{1, -\frac{1}{2}, -100, 1\}$ $\{1, -2, -\frac{1}{100}, \mathrm{Im}, \mathrm{Im}, 0.1, -1, 0.201\}$, (j) $\{\frac{1}{3}, -\frac{1}{2}, -100, 1\}\{3, -2, -\frac{1}{300}, \mathrm{Im}, -0.002\,36, \mathrm{Im}, 1, \frac{601}{300}\}$, (k) $\{-1, 2, -1, 1\}\{-1, \frac{1}{2}, 1, \mathrm{Im}, 1, \mathrm{Im}, -2, -1.5\}$, (m) $\{-1, 2, -100, 1\}$ $\{-1, \frac{1}{2}, 0.01, \mathrm{Im}, 0.01, \mathrm{Im}, -2, -0.51\}$, (n) $\{-2, 1, -1, 1\}\{-0.5, 1, 2, \mathrm{Im}, \mathrm{Im}, 1., 2, -3\}$, and (p) $\{-2, 1, -100, 1\}\{-0.5, 1, \frac{1}{50}, \mathrm{Im}, \mathrm{Im}, 0.1, 2, -\frac{51}{50}\}$.

C. Impedance characterization of stability and bifurcation

The Jacobian (11) can be written in terms of the equivalent circuit elements as

$$\begin{pmatrix} -\dfrac{1}{R_b C_m} & -\dfrac{1}{C_m} \\ \dfrac{1}{L_a} & -\dfrac{L_a}{R_a} \end{pmatrix}. \tag{32}$$

The condition $T_\lambda = 0$ for the Hopf bifurcation is

$$\frac{R_a}{L_a} = -\frac{1}{R_b C_m}. \tag{33}$$

The existence of Hopf bifurcation requires that at least one of the elements R_b, R_a, or L_a is negative to satisfy Eq. (33). (One or three elements can be negative but not only two at the same time.)

The stability analysis is often done in terms of the zeros and poles of the impedance.[52] Let us write Eq. (19) as

$$Z(s) = \frac{R_I}{\tau_u} \frac{s+\omega_L}{(s+\omega_b)(s+\omega_L)+\omega_a\omega_L}. \tag{34}$$

In galvanostatic operation, the Hopf bifurcations are given by the poles of the impedance, i.e., the zeros of the admittance $Y = Z^{-1}$ at a finite frequency.[10] The denominator of Eq. (34) corresponds to the characteristic equation (12), whose zeroes are the eigenvalues. Hence, the poles correspond to the condition $\lambda = i\omega_o$ that determines the Hopf bifurcation.[4,5] It is satisfied when

$$\omega_L = -\omega_b, \tag{35}$$

or alternatively,

$$\omega_d = \omega_o. \tag{36}$$

Both these conditions correspond to Eq. (33).

The transition of the impedance spectra across the Hopf bifurcation starts from the stable spectrum in Fig. 7(b). Close to the bifurcation (in the stable side), the impedance develops a small real negative part, Figs. 3(b) and 7(c). At the bifurcation, the impedance crosses the origin at a finite frequency. Then, the intercept of the real axis passes to negative values as in Figs. 1(b) and 7(d). This last spectrum indicates the voltage oscillations as shown in Fig. 1(e), and ω_o is the frequency of the oscillations.[56] The sequence of the spectra is illustrated in Fig. 5 and in a video presented in the supplementary material.

A negative resistance sector in R_b is a frequent mechanism of spontaneous oscillations. For example, in the FHN model, there is a range of $R_b < 0$. Since $R_{dc} > 0$ and $R_b < 0$ in Fig. 1(b), this impedance pattern is termed by Koper and Sluyters, the "negative hidden resistance."[48] The causes for the occurrence of a negative differential resistance have been reviewed.[11]

In the saddle-node bifurcation, R_{dc} crosses the origin at zero frequency from positive to negative values. The negative dc resistance spectra 7e, g, h, k, and m indicate the unstable condition $\Delta < 0$ provided that (25) is satisfied.

For the potentiostatic oscillations, a series resistance is necessary, not included in Fig. 7. This mode will be discussed in Sec. V. When the voltage is fixed, the Hopf bifurcation occurs when the impedance is zero at finite frequency or equivalently by the poles of the admittance function.[10] These conclusions can be obtained by the general analysis of Koper based on the Nyquist stability criterion.[57]

As the stability conditions and the shape of the spectra are established by the relative values of the characteristic frequencies $\omega_a, \omega_b, \omega_L, \omega_c, \omega_d$, and ω_o, a plot of the frequencies with respect to voltage produces a full characterization of impedance spectra and dynamical properties. The code of colors and general properties of the characteristic frequencies are presented in Table I and summarized in Table II, and examples are shown in Figs. 4(b) and 8(c). The oscillation frequency ω_o is shown only in regions of self-sustained oscillations.

IV. THE PARALLEL MODEL: OSCILLATING SYSTEMS AT CONSTANT CURRENT

A. The FitzHugh–Nagumo neuron model

Dynamical models for neuronal responses are formed by a nonlinear set of dynamical equations that emulate the actual output of a biological neuron.[42,58,59] The HH model[21] is formed by the membrane capacitance and several voltage-dependent conductance that describes the activation and deactivation of different ion channels. IS of the HH model shows correspondingly a complex response,[20,30,60–62] and here, we restrict the analysis to minimal dynamical models composed of a two-dimensional system that contains the evolution of the membrane potential u and a slower recovery variable.[38] The first minimal model was developed by FitzHugh[63] and Nagumo *et al.*[59] by reducing the three slow variables of the HH model to just one refractory current.[38,43–45,64–69]

Here, we consider the recent results of IS in relation to dynamical properties.[34] The bifurcation conditions in FHN are expressed by parameters ε, r, b (Table I). The line $r = b$ is a pitchfork bifurcation. $r/b > 1$ corresponds to the single valued $I - u$ with a positive R_{dc}. The model realization shown in Fig. 8 is the same as those of Figs. 1, 2(b), 2(c), and 3. In Fig. 8, we show the stability plots, the resistances and inductor, and the characteristic frequencies. As $T_\lambda > 0$ in Fig. 8(a) is the region of limit cycle oscillations, the borders of this regions are Hopf bifurcations as indicated by red points in Fig. 8(c).

We examine the impedance and dynamical regimes. Figure 1 is for a fixed current at $u = 0.7$ that falls into the oscillation region in the frequency diagram, as shown in Fig. 8(c). The impedance spectrum

TABLE II. Classification of dynamical properties by the plots of stability properties and characteristic frequencies.

Properties	Stability graph vs u	Frequencies graph vs u
Positive R_{dc}	Red > 0	Red > 0
Hopf bifurcation	Red > 0, intercept of brown and u axis	Red > 0, intercept blue and purple
Self-sustained oscillations	Red > 0, brown > 0	Red > 0, blue > purple
Inductive loop in impedance		Orange > 0, blue < purple
Crossing the vertical axis of the impedance		Gray > 0

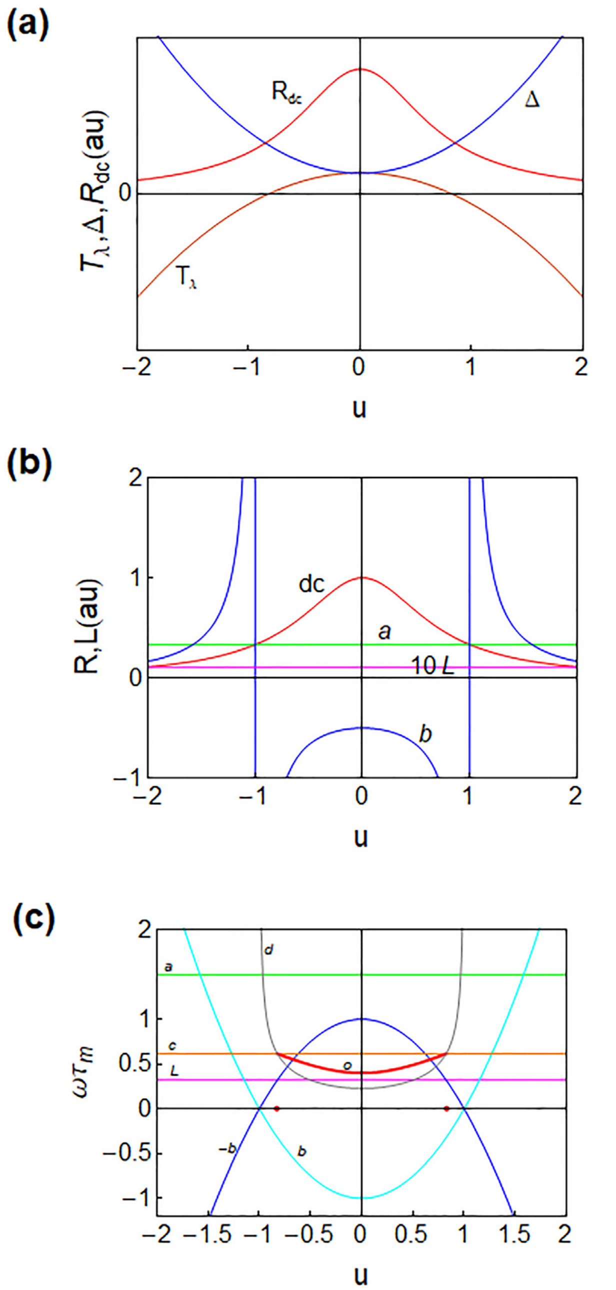

FIG. 8. Representation of quantities as a function of voltage for the FitzHugh–Nagumo model with parameters $R_l = 0.5$, $b = 0.8$, $r = 1.2$, $\epsilon = 0.4$, and $\tau_m = 0.01$. The code of colors is indicated in Table I. (a) Stability quantities. (b) Resistances and inductor. (c) Characteristic frequencies. The frequency of oscillations ω_o is indicated only in the region of oscillation between two Hopf bifurcations, shown by red points at $u_H = \pm 0.8246$.

is that of a hidden negative resistance with the intercept at the frequency ω_c in the negative real axis, Fig. 1(b). The associated motion in the phase plane in Fig. 1(c) is a limit cycle around the fixed point at $u = 0.7$. The spikes with frequency ω_o are shown in Fig. 1(e). In contrast to this behavior, at the voltage $u = 0.9$, Fig. 3, the system reaches a stable steady state. Since $\omega_c > 0$, as shown in Fig. 8(c), the impedance shows an inductive hook, Fig. 3(b), and the corresponding trajectory produces an overdamped oscillation of the voltage. The gray line in Fig. 8(c) indicates that the impedance crosses the vertical axis as in Fig. 3(b), which happens when $\omega_b = 0$.

We turn to another set of parameters, $r/b < 1$, that cause $\Delta < 0$ with a region of negative R_{dc}, Fig. 9. The fixed current intercepts $I - u$ at three points, a saddle, and two sinks. The saddle state B is clearly unstable, but the system may evolve with time to A or C depending on the nature of these fixed points. Since point C is situated in a potential lower than the Hopf bifurcation, it is unstable. Hence, the perturbed system will arrive to point A for any possible initial condition, as shown in Figs. 10(a) and 10(b). Now, the local impedance indicating oscillations in Fig. 10(e) is not able to describe the global trajectory since the system chooses another destiny point. Figure 4 is presented another set of FHN parameters. Now, point C at $u = 0.85$ is stable, and the trajectory in Fig. 4(c) is a damped oscillation to C as predicted by the inductive hook in the impedance spectrum in Fig. 4(e). However, a small change in the initial perturbation moves the trajectory to the basin of attraction of point A, as shown in Fig. 4(d), and again the local impedance does not describe the global trajectory.

B. The Koper–Sluyters (KS) electrochemical model

The properties of electrochemical oscillators have been classified,[17] and the bifurcations and different regimes of oscillations are well described by the impedance spectra.[10–12,15,16,18,46–48,56,57,70–74] We characterize the impedance and dynamical regimes in a representative model due to Koper and Sluyters[48] for an electrochemical reaction with a potential dependent absorption rate that includes Hopf bifurcation. It is described by the following functions:

$$f = -k_e(u)x + I_{tot}, \tag{37}$$

$$g = \mathrm{k}_a(u)(1 - x) - k_e(u), \tag{38}$$

and $\tau_u = \epsilon$, $\tau_k = 1$. The physical variables are the electrode potential u, the external current I_{tot}, and a surface absorption variable $0 \le x \le 1$. In the steady state,

$$x = \frac{k_a}{k_a + k_e}, \tag{39}$$

$$I_{tot} = k_e x = \frac{k_a k_e}{k_a + k_e}. \tag{40}$$

For $k_e(u)$, it is assumed an N-shaped function,

$$k_e(u) = \frac{k_{e1}^0 \exp(f\alpha u)}{1 + k_d \exp[fb_2(u - u_d)]} + k_{e2}^0 \exp(f\alpha u). \tag{41}$$

For $k_a(u)$, a sigmoidal function is adopted,

$$k_a(u) = \frac{1}{1/[k_a^0 \exp[fb_1(u - u_a)] + 1/k_m}. \tag{42}$$

The bifurcation behavior according to parameter ranges are explained in the original reference by KS.[48] Here, we describe the case of Fig. 11(a) in which the negative resistance is visible in the $I - u$ curve (see Fig. 5). Now, we provide a detailed characterization of

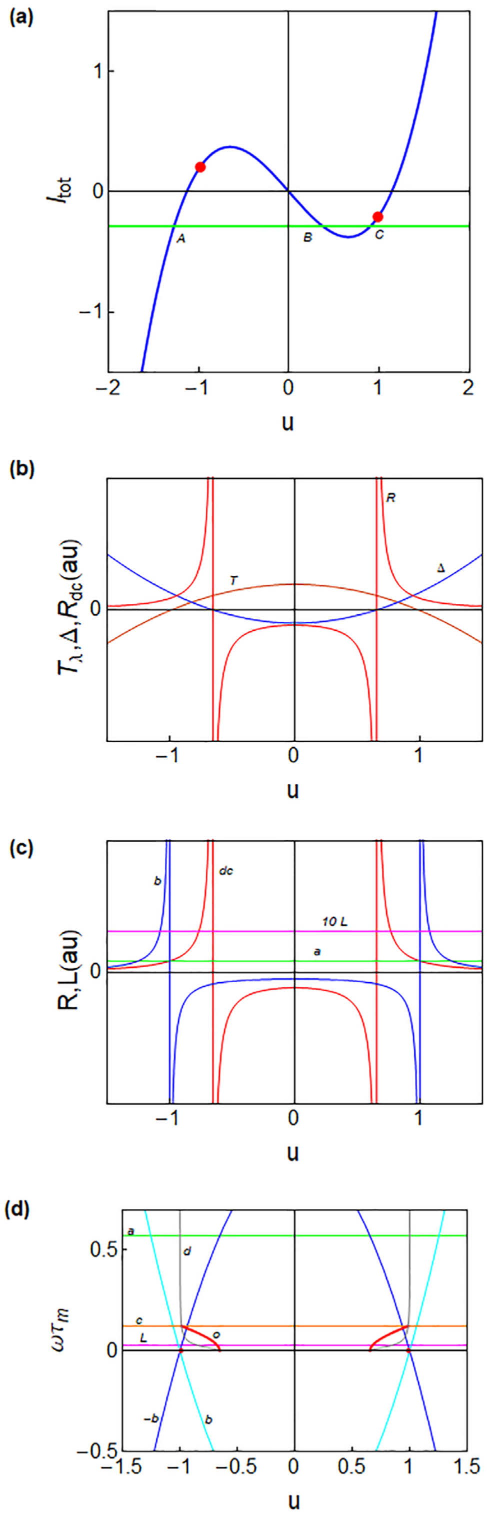

FIG. 9. FitzHugh–Nagumo model for $R_l = 0.5$, $b = 1.4$, $r = 0.8$, $\epsilon = 0.02$, $\tau_m = 0.01$, and $u_H = 0.9860$. (a) Current–voltage curve. (b) Stability quantities. (c) Resistances and inductor. (d) Characteristic frequencies.

impedance spectra and associated trajectories by analysis of the frequency graph Fig. 11(d). We note that this system is more complex that the previously discussed FHN, since all the characteristic frequencies in the KS model depend on the voltage. The following impedance characteristics can be observed in Fig. 11(d). The letters in parentheses correspond to Fig. 7.

$u = 0 - 0.190$: single positive arc (a).

$u = 0.190 - 0.226$: hook feature with resistances in the positive axis (orange positive), (b). close to the Hopf bifurcation, at the onset of the gray line, a negative real part of the impedance develops (c).

$u = 0.226 - 0.321$: Hidden negative resistance spectrum with the intercept at the negative x axis (d). This is the oscillatory regime shown in Fig. 12.

$u = 0.334 - 0.400$: negative dc resistance with double arc feature (g).

$u = 0.400 - 0.500$: The inductor becomes negative, see Fig. 11(e), but ω_L is positive and ω_c is not a real number; hence, the spectrum is first a single positive arc (n) that becomes a double arc (p).

These results are illustrated in motion in a video presented in the supplementary material.

V. THE SERIES MODEL: OSCILLATION AT CONSTANT VOLTAGE

In a system of the type of Fig. 6, a fixed voltage will prevent any periodic oscillation. However, most electrical systems have a resistance in series due to the characteristics of the contacts. Once the series resistance R_s is added, the voltage applied to the system V is divided into two components,

$$V = I_{tot} R_s + u, \tag{43}$$

where I_{tot} is the external current and u is the voltage in the main subcircuit. Now, there can be oscillations of the internal voltage u, as is described in electrochemistry[10–12,70] and semiconductor devices.[40,75] By the addition of Eq. (43) to the systems of Sec. III, the oscillations at fixed voltage can be obtained. However, the circuit of Fig. 6 is then not a minimal model. The reason for this is that the series resistance can stabilize the negative resistance; hence, it is possible to remove the R_b line and instead situate the negative resistance in R_a. To illustrate the impedance of a such a system for potentiostatic oscillations, we use a model described in Sec. VI B of Schöll's book.[40] The system consists of a circuit with capacitive current and conduction current i_c (the slow stabilizing variable),

$$I_{tot} = C_m \frac{du}{dt} + i_c. \tag{44}$$

The branch with conduction current is formed by an inductor and a nonlinear element with voltage u_c and characteristic conduction function $u_c(i_c)$, which includes a negative resistance behavior. We, therefore, have

$$C_m \frac{du}{dt} = -\frac{u}{R_s} - i_c + \frac{V}{R_s}, \tag{45}$$

$$L_a \frac{di_c}{dt} = u - u_c(i_c). \tag{46}$$

These equations can be generalized to the form (1) and (2) with V instead of I_{tot}, producing a series rather than parallel connection.

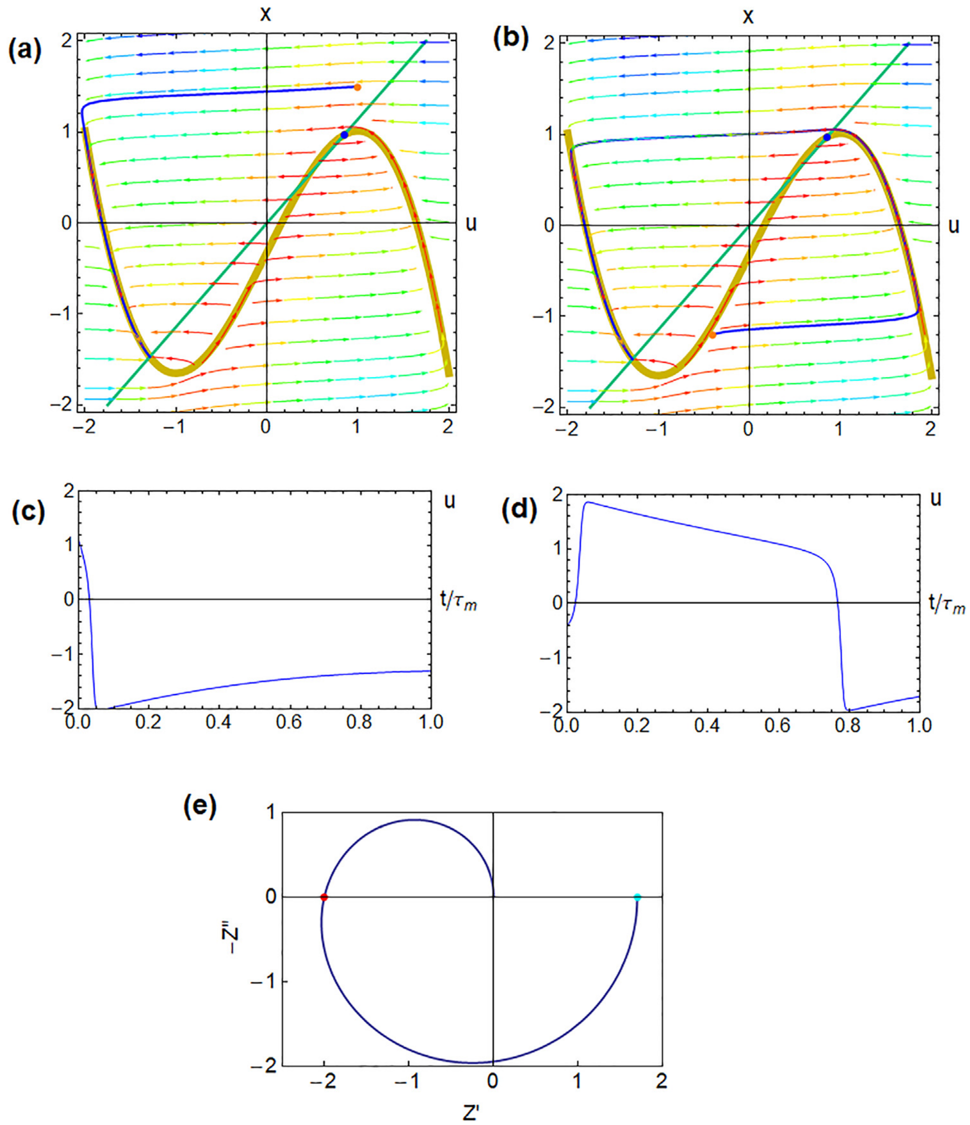

FIG. 10. A FHN model behavior, same parameters of Fig. 9, in point C of the $I-u$ curve. (a)–(c) Phase portraits and (c) and (d) voltage oscillations starting from different points. (e) Impedance spectrum, indicating the characteristic frequencies $\omega = 0$ (cyan) and the crossing of the horizontal axis (red, ω_c). Parameters: $R_l = 0.5$, $b = 1.4$, $r = 0.8$, $\epsilon = 0.02$, $\tau_m = 0.01$, $u = 0.85$ (point C), $\{R_a, R_b, L_a, C_m\} = \{0.875, -2.631, 0.3125, 0.02\}$, and $\{\omega_a, \omega_b, \omega_L, \omega_c, \omega_o, R_{dc}, -\omega_L - \omega_b\} = \{57.1, -19.0, 2.80, 12.3, 10.3, 1.31, 16.2\}$.

The linearized and Laplace transformed variables have the form

$$\hat{V} = \hat{I}_{tot} R_s + \hat{u}, \tag{47}$$

$$C_m s\hat{u} = -\frac{\hat{u}}{R_s} - \hat{i}_c + \frac{\hat{V}}{R_s}, \tag{48}$$

$$L_a s\hat{i}_c = \hat{u} - R_a \hat{i}_c, \tag{49}$$

where

$$R_a = \frac{du_c}{di_c}. \tag{50}$$

The impedance function $\hat{V}/\hat{I}_{tot}$ has the following form:

$$Z(s) = R_s\left(1 + \frac{\omega_s}{s + \dfrac{\omega_a}{1 + \dfrac{s}{\omega_L}}}\right). \tag{51}$$

The frequencies are

$$\omega_a = \frac{1}{R_a C_m}, \tag{52}$$

$$\omega_s = \frac{1}{R_s C_m}, \tag{53}$$

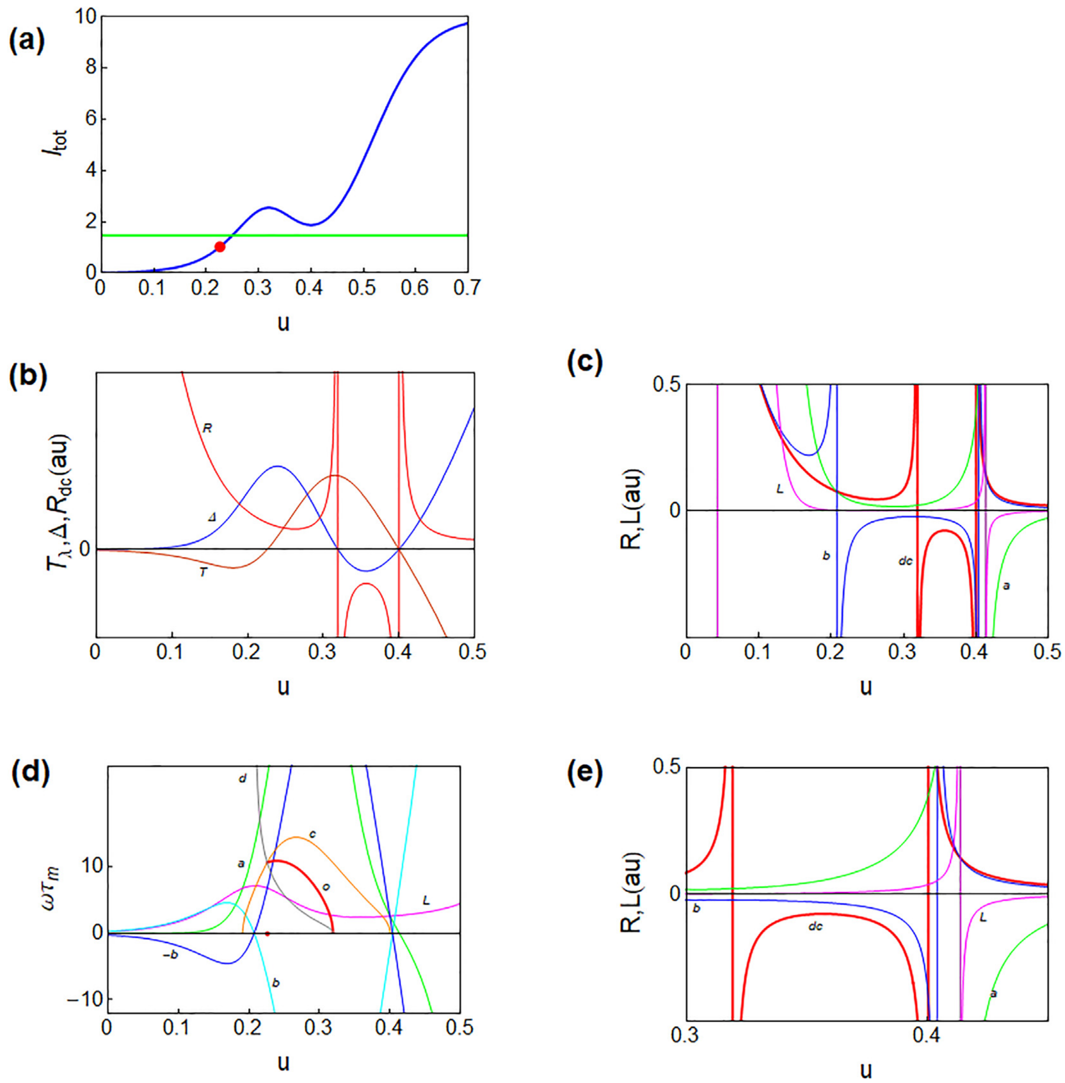

FIG. 11. Koper–Sluyters model for $\epsilon = 0.25$, $\tau_m = \epsilon$, $k_{e1} = 1$, $\alpha = 0.5$, $f = 38.7$, $k_d = 250$, $b_2 = 1$, $k_{a0} = 0.015$, $b_1 = 0.5$, $k_m = 10$, $u_a = 0$, $u_d = 0.35$, $k_{e2} = 0.0005$, $u_H = 0.226$, and $u = 0.25$. (a) Current–voltage, (b) stability graph, (c) resistances and inductor, (d) frequencies graph, and (e) detail of (c) showing the change of sign of the inductor.

$$\omega_L = \frac{R_a}{L_a}. \tag{54}$$

The system can be represented by the small ac impedance equivalent circuit of Fig. 13.

The Jacobian is similar to (32),

$$\begin{pmatrix} -\omega_s & -\dfrac{1}{C_m} \\ \dfrac{1}{L_a} & -\omega_L \end{pmatrix}. \tag{55}$$

The trace and determinant have the values,

$$T_\lambda = -\omega_s - \omega_L, \tag{56}$$

$$\Delta = \omega_L(\omega_s + \omega_a). \tag{57}$$

According to Eq. (56), the oscillation region $T_\lambda > 0$ requires that either R_a or L_a become negative, but not at the same time. The oscillation frequency is

$$\omega_o = [\omega_L(\omega_s + \omega_a)]^{1/2}. \tag{58}$$

We investigate here an S-shaped characteristic of the type,

$$u_c = R_w\left(\frac{i_c^3}{3} - i_c\right), \tag{59}$$

where R_w is a constant resistor. The current–voltage curve is

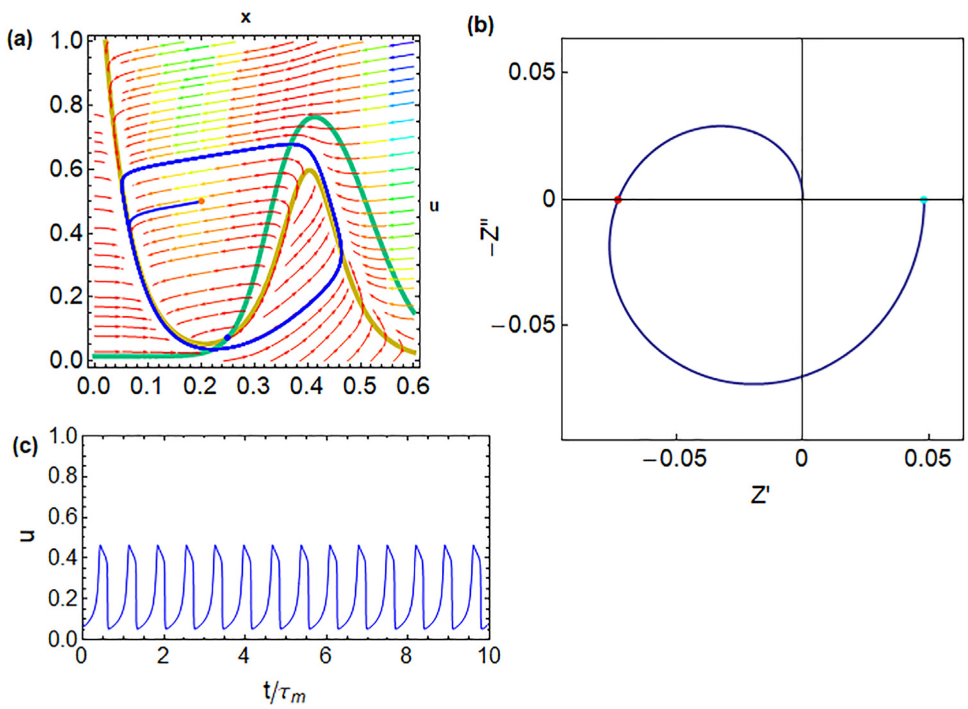

FIG. 12. Oscillatory behavior of the Koper–Sluyters model, same parameters as Fig. 11. (a) Trajectory in the phase plane. (b) Impedance spectrum, indicating the characteristic frequencies $\omega = 0$ (cyan) and the crossing of the horizontal axis (red, ω_c). (c) Voltage oscillations.

$$V_{dc} = R_s I_{dc} + R_w\left(\frac{I_{dc}^3}{3} - I_{dc}\right). \tag{60}$$

The dc resistance gives

$$R_{dc} = \frac{R_s}{r}\left(r - 1 + I_{dc}^2\right), \tag{61}$$

where

$$r = \frac{R_s}{R_w}. \tag{62}$$

The intercept with the real axis $Z'' = 0$ is at the frequency

$$\omega_c = [\omega_L(\omega_a - \omega_L)]^{1/2} \tag{63}$$

and the intercept with the imaginary axis $Z'' = 0$ is at

$$\omega_d = \left\{\frac{1}{2}\omega_L\left[2\omega_a - \omega_L + \left(\omega_L^2 - 4\omega_a\omega_L - 4\omega_a\omega_s\right)^{\frac{1}{2}}\right]\right\}^{1/2}. \tag{64}$$

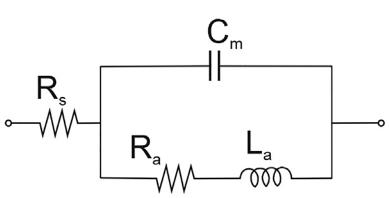

FIG. 13. Equivalent circuit for the series model.

TABLE III. Series circuit: Model parameters and derived quantities.

Parameters/variables	Code	Equivalent circuit
C_m		
R_a		$\frac{du_c}{di_c}$
R_s		
L_a		
R_{dc}		$R_s + R_a$
ω_a		$\frac{1}{R_a C_m}$
ω_s		$\frac{1}{R_s C_m}$
$-\omega_s$		
ω_L		$\frac{R_a}{L_a}$
ω_c Z crossing the real axis		$[\omega_L(\omega_a - \omega_L)]^{1/2}$
Z_1' Impedance at crossing real axis		$R_s + \frac{L_a}{R_a C_m}$
ω_d Z crossing the imaginary axis		
Δ		$\omega_L(\omega_s + \omega_a)$
ω_o		$[\omega_L(\omega_a + \omega_s)]^{1/2}$
T_λ(oscillation if $T_\lambda > 0$)		$-\omega_s - \omega_L$
u_{Hopf}		$\frac{R_a R_s C_m}{L_a} = -1$
$\omega_s = -\omega_L$		

The results are summarized in Table III. As remarked earlier, the presence of potentiostatic oscillations after Hopf bifurcation requires that the admittance crosses the origin of the complex plane at finite frequency.[57] Accordingly, in Fig. 14, we plot the different impedance patterns by the combinations of characteristic frequencies, and the correspondent admittance pattern is shown in Fig. 15.

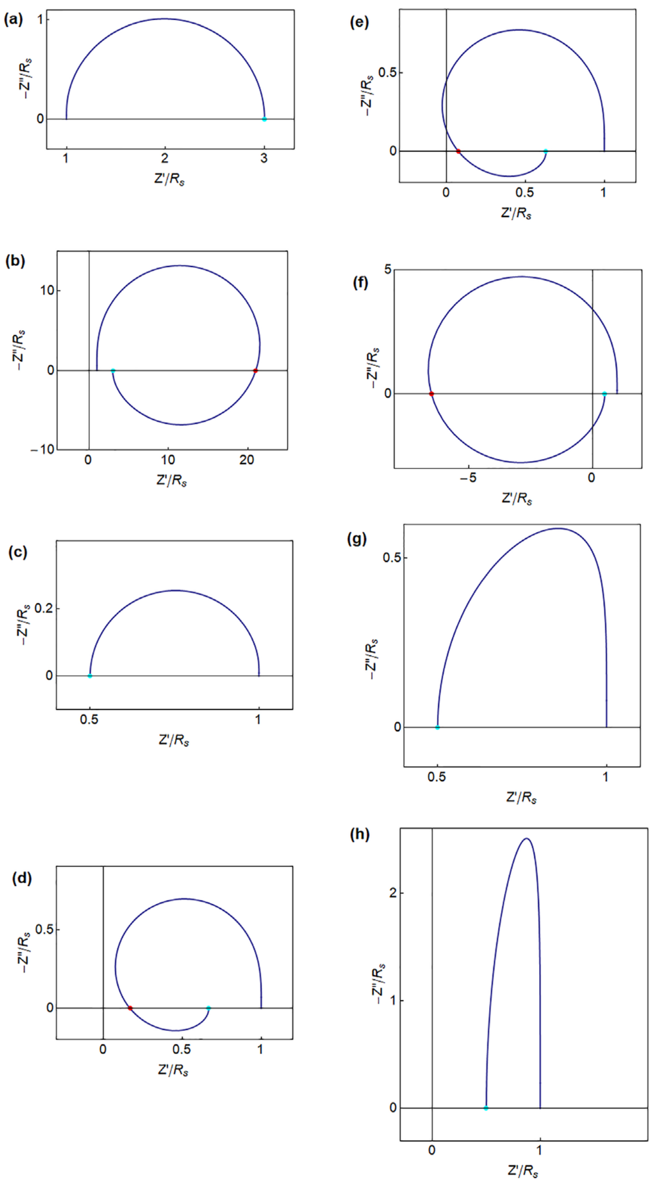

FIG. 14. Complex plane impedance plot representation of the spectral patterns of the impedance model in Fig. 13, indicating the characteristic frequencies $\omega = 0$ (cyan) and the crossing of the horizontal axis (red, ω_c). Parameters: $\{R_a, R_s, L_a, C_m\}\{\omega_a, \omega_s, \omega_L, \omega_c, \omega_d, \omega_o, R_{dc}, -\omega_L - \omega_b\}$ (a) $\{0.5, 1, 0.1, 1\}\{1, 2., 10., Im, Im, 5.48, 1.5, -12\}$, (b) $\{0.5, 1, 10, 1\}\{1, 2, \frac{1}{10}, 0.3, Im, 0.547, 1.5, -2.1\}$, (c) $\{2, -1, 0.1, 1\}\{-1, \frac{1}{2}, -10, Im, Im, 2.24, 1, 9.5\}$, (d) $\{6, -2, 10, 1\}\{-\frac{1}{2}, \frac{1}{6}, -\frac{1}{5}, Im, 0.258, 4, \frac{1}{30}\}$, (e) $\{5.4, -2, 10, 1\}\{-\frac{1}{2}, 0.185, -\frac{1}{5}, 0.245, 0.300, 0.251, 3.40, 0.0148\}$, (f) $\{2, -1, 15, 1\}\{-1, \frac{1}{2}, -\frac{1}{15}, 0.249, 0.329, 0.182, 1, -\frac{13}{30}\}$, (g) $\{2, -1 - 5, 1\}\{-1, \frac{1}{2}, \frac{1}{5}, Im, Im, Im, 1, -\frac{7}{10}\}$, and (h) $\{2, -1, -100, 1\}\{-1, \frac{1}{2}, \frac{1}{100}, Im, Im, Im, 1, -\frac{51}{100}\}$.

Figure 16 shows the stability, resistances, and characteristic frequencies plots of the series model outlined above. The following impedance characteristics and the correspondent admittance spectra can be observed in Fig. 16(c). The letters in parentheses correspond to Fig. 14.

$I_{dc} = 0 - 0.240$: single positive arc with $R_{dc} > R_s$ (c). Oscillations (up to the Hopf bifurcation) by magenta < blue, as shown in Fig. 16(e).

$I_{dc} = 0.240 - 0.550$: arc with inductive features (d).

$I_{dc} = 0.550 - 0.632$: Intercept with the vertical axis (e). The arc grows, Fig. 16(g), and the intercept with the x-axis passes the origin to negative values at the Hopf bifurcation.

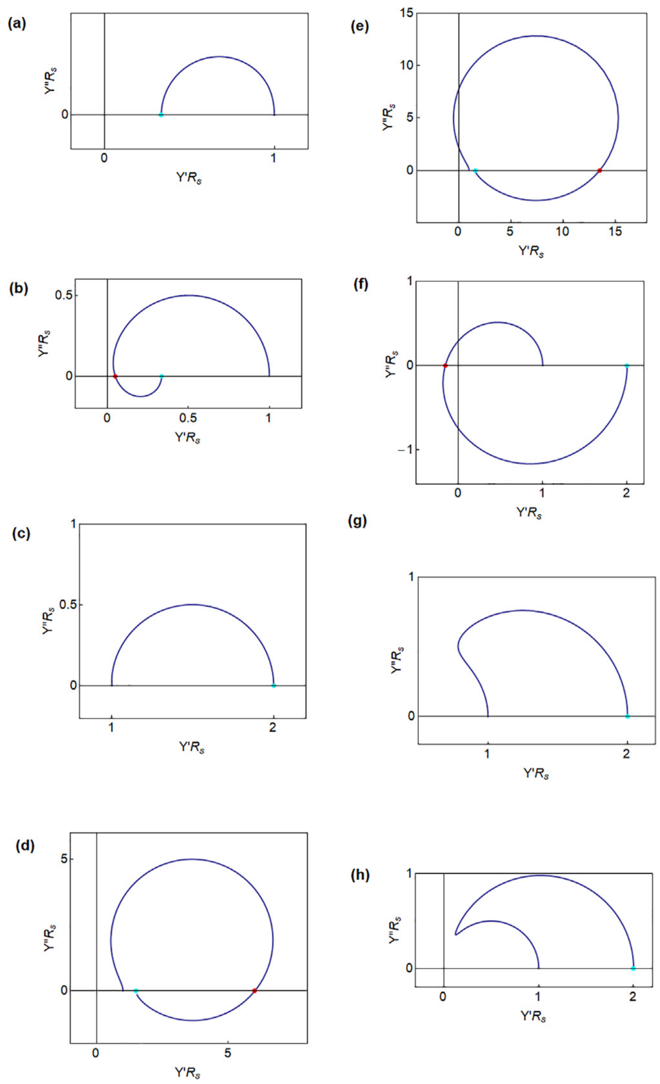

FIG. 15. Complex plane admittance plot representation of the spectral patterns of the impedance model in Fig. 13, indicating the characteristic frequencies $\omega = 0$ (cyan) and the crossing of the horizontal axis (red, ω_c). The same parameters as Fig. 14.

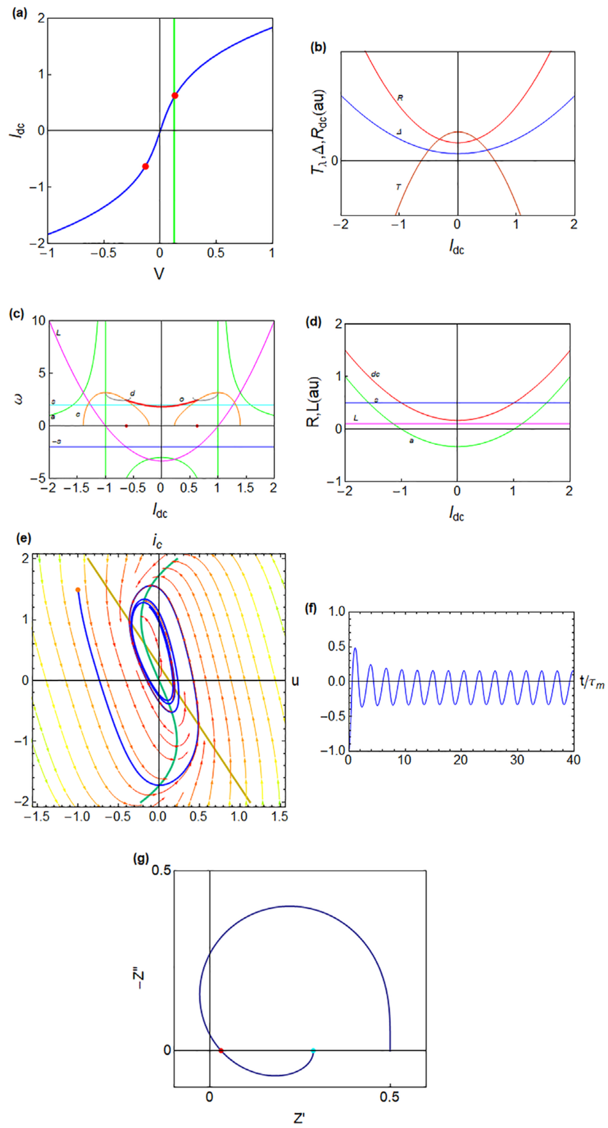

FIG. 16. Dynamical properties of Schöll's series model. (a) Current–voltage curve. The Hopf bifurcation is at $I_H = 0.632$. The green line is the voltage at $I_{tot} = 0.600$, close to the Hopf bifurcation in the oscillatory side. (b) Stability graph; (c) frequencies graph; (d) resistances and inductor; and (e) nullclines, trajectories, and vector velocities. The line is the $\dot{u} = 0$ nullcline, and the yellow line is the $\dot{i}_c = 0$ nullcline. The blue point is the fixed point at the nominal potential. The orange point is the starting condition. Color streamlines indicate the norm of the vector field. (f) Voltage evolution with time. (g) Impedance spectrum, indicating the characteristic frequencies $\omega = 0$ (cyan) and the crossing of the horizontal axis (red, ω_c). The Hopf bifurcation occurs when the red point arrives to the origin. Parameters: $R_s = 0.5, r = 1.5, L_a = 0.1, C_m = 1, I_{tot} = 0.6,\ \{R_a, R_s, L_a, C_m\} = \{-0.318, 0.5, 0.1, 1\}$, and $\{\omega_a, \omega_b, \omega_L, \omega_c, \omega_o, R_{dc}, -\omega_L - \omega_b\} = \{-3.14, 2, -3.18, -0.133, Im, 1.906, 0.197, 1.18\}$.

$I_{dc} = 0.632 - 1.00$: Pattern (f).

$I_{tot} = 1.00 - 1.40$: R_{dc} increases until the gray line disappears. At this point, the arc passes to the positive x-axis (b).

$I_{tot} = 1.40 - 2.00$: The inductive feature (orange line) vanishes to pattern (a).

VI. CONCLUSIONS

In the models and experimental analysis of the impedance spectra of oscillating current–voltage systems, there occurs a fascinating succession of very different shapes that describe the changing dynamical properties. We have analyzed a general fast–slow model leading to a Hopf bifurcation and several specific models to interpret the meaning of the impedance in terms of temporal dynamic characteristics. We devised a new general method based on characteristic frequencies that appear naturally in the impedance function and by the stability conditions, which provides a visual map of the succession of impedance forms and dynamic regimes. The method classifies all the behaviors in a two-dimensional fast–slow system, and, hopefully, it can be extended to deal with more complex situations such as the Hodgkin–Huxley model.

SUPPLEMENTARY MATERIAL

See the supplementary material for the Mathematica program to calculate the graphs and a video with animated cartoons to explain the evolution of impedances by the map of characteristic frequencies, https://youtu.be/rTGfSfKLuDk (Ref. 76).

ACKNOWLEDGMENTS

We thank financial support by Ministerio de Ciencia e Innovación of Spain (MICINN) under Project No. PID2019-107348GB-100.

AUTHOR DECLARATIONS

Conflict of Interest

The author has no conflicts to disclose.

DATA AVAILABILITY

Data sharing is not applicable to this article as no new data were created or analyzed in this study.

REFERENCES

[1] *The Hopf Bifurcation and its Applications*, edited by J. E. Marsden and M. McCracken (Springer-Verlag, 1976).

[2] M. Eiswirth, A. Freund, and J. Ross, "Mechanistic classification of chemical oscillators and the role of species," Adv. Chem. Phys. **80**, 127–199 (1991).

[3] S. K. Scott, *Chemical Chaos* (Clarendon Press, 1991).

[4] J. Guckenheimer, M. Myers, and B. Sturmfels, "Computing Hopf bifurcations I," SIAM J. Sci. Comput. **34**, 1–21 (1991).

[5] J. Guckenheimer and M. Myers, "Computing Hopf bifurcations. II: Three examples from neurophysiology," SIAM J. Sci. Comput. **17**, 1275–1301 (1996).

[6] S. H. Strogatz, *Nonlinear Dynamics and Chaos*, 2nd ed. (CRC Press, 2019).

[7] A. Lasia, *Electrochemical Impedance Spectroscopy and its Applications* (Springer, 2014).

[8] A. Guerrero, J. Bisquert, and G. Garcia-Belmonte, "Impedance spectroscopy of metal halide perovskite solar cells from the perspective of equivalent circuits," Chem. Rev. **121**, 14430–14484 (2021).

[9] M. E. Orazem and B. Tribollet, *Electrochemical Impedance Spectroscopy*, 2nd ed. (Wiley, 2017).

[10] M. T. M. Koper, "Non-linear phenomena in electrochemical systems," J. Chem. Soc., Faraday Trans. **94**, 1369–1378 (1998).

[11] K. Krischer, "Nonlinear dynamics in electrochemical systems," in *Advances in Electrochemical Science and Engineering, Vol. 8*, edited by R. C. Alkire and D. M. Kolb (Wiley, 2002), pp. 89–208.

[12] M. Orlic, *Self-Organization in Electrochemical Systems I* (Springer, 2012).

[13]M. T. M. Koper, E. A. Meulenkamp, and D. Vanmaekelbergh, "Oscillatory behavior of the hydrogen peroxide reduction at gallium arsenide semiconductor electrodes," J. Phys. Chem. **97**, 7337–7341 (1993).
[14]M. T. M. Koper and D. Vanmaekelbergh, "Stability study and categorization of electrochemical oscillators by impedance spectroscopy," J. Phys. Chem. **99**, 3687–3696 (1995).
[15]F. Berthier, J.-P. Diard, and C. Montella, "Hopf bifurcation and sign of the transfer resistance," Electrochim. Acta **44**, 2397 (1999).
[16]V. V. Pototskaya, O. I. Gichan, A. A. Omelchuk, and S. V. Volkov, "Specific features of the behavior of an electrochemical system in the case of the Hopf instability for a spherical electrode," Russ. J. Electrochem. **44**, 594–601 (2008).
[17]P. Strasser, M. Eiswirth, and M. T. M. Koper, "Mechanistic classification of electrochemical oscillators—An operational experimental strategy," J. Electroanal. Chem. **478**, 50–66 (1999).
[18]F. Berthier, J.-P. L. Diard, B. Gorrec, and C. Montella, "Discontinuous immittance due to a saddle node bifurcation. I. 1-, 2- and 3-part immittance diagrams," J. Electroanal. Chem. **458**, 231–240 (1998).
[19]L. Lapicque, "Recherches quantitatives sur l'excitation electrique des nerfs traitée comme une polarization," J. Physiol. Pathol. Gen. **9**, 620–635 (1907).
[20]K. S. Cole and R. F. Baker, "Longitudinal impedance of the squid giant axon," J. Gen. Physiol. **24**, 771–788 (1941).
[21]A. L. Hodgkin and A. F. Huxley, "A quantitative description of membrane current and its application to conduction and excitation in nerve," J. Physiol. **117**, 500–544 (1952).
[22]B. S. Pallotta and P. K. Wagoner, "Voltage-dependent potassium channels since Hodgkin and Huxley," Physiol. Rev. **72**, S49–S67 (1992).
[23]Y. Tuchman, T. N. Mangoma, P. Gkoupidenis, Y. van de Burgt, R. A. John, N. Mathews, S. E. Shaheen, R. Daly, G. G. Malliaras, and A. Salleo, "Organic neuromorphic devices: Past, present, and future challenges," MRS Bull. **45**, 619–630 (2020).
[24]Y. van de Burgt and P. Gkoupidenis, "Organic materials and devices for brain-inspired computing: From artificial implementation to biophysical realism," MRS Bull. **45**, 631–640 (2020).
[25]M. Javad, M. Hossein, E. Donati, T. Yokota, S. Lee, G. Indiveri, T. Someya, and R. A. Nawrocki, "Organic electronics Axon-Hillock neuromorphic circuit: Towards biologically compatible, and physically flexible, integrate-and-fire spiking neural networks," J. Phys. D: Appl. Phys. **54**, 104004 (2021).
[26]R. A. John, N. Tiwari, M. I. B. Patdillah, M. R. Kulkarni, N. Tiwari, J. Basu, S. K. Bose, A. Ankit, C. J. Yu, A. Nirmal, S. K. Vishwanath, C. Bartolozzi, A. Basu, and N. Mathews, "Self healable neuromorphic memtransistor elements for decentralized sensory signal processing in robotics," Nat. Commun. **11**, 4030 (2020).
[27]K. Kang, W. Hu, and X. Tang, "Halide perovskites for resistive switching memory," J. Phys. Chem. Lett. **12**, 11673–11682 (2021).
[28]K. J. Kwak, D. E. Lee, S. J. Kim, and H. W. Jang, "Halide perovskites for memristive data storage and artificial synapses," J. Phys. Chem. Lett. **12**, 8999–9010 (2021).
[29]H. J. Gogoi, K. Bajpai, A. T. Mallajosyula, and A. Solanki, "Advances in flexible memristors with hybrid perovskites," J. Phys. Chem. Lett. **12**, 8798–8825 (2021).
[30]A. Bou and J. Bisquert, "Impedance spectroscopy dynamics of biological neural elements: From memristors to neurons and synapses," J. Phys. Chem. B **125**, 9934–9949 (2021).
[31]M. Rahimi Azghadi, Y.-C. Chen, J. K. Eshraghian, J. Chen, C.-Y. Lin, A. Amirsoleimani, A. Mehonic, A. J. Kenyon, B. Fowler, J. C. Lee, and Y.-F. Chang, "Complementary metal-oxide semiconductor and memristive hardware for neuromorphic computing," Adv. Intell. Syst. **2**, 1900189 (2020).
[32]A. Mehonic and A. J. Kenyon, "Emulating the electrical activity of the neuron using a silicon oxide RRAM cell," Front. Neurosci. **10**, 57 (2016).
[33]J. Gong, H. Wei, Y. Ni, S. Zhang, Y. Du, and W. Xu, "Methylammonium halide-doped perovskite artificial synapse for light-assisted environmental perception and learning," Mater. Today Phys. **21**, 100540 (2021).
[34]J. Bisquert, "A frequency domain analysis of excitability and bifurcations of Fitzhugh-Nagumo neuron model," J. Phys. Chem. Lett. **12**, 11005–11013 (2021).
[35]G. Innocenti, M. Di Marco, A. Tesi, and M. Forti, "Memristor circuits for simulating neuron spiking and burst phenomena," Front. Neurosci. **15**, 681035 (2021).
[36]M. D. Marco, M. Forti, G. Innocenti, A. Tesi, and F. Corinto, "Targeting multistable dynamics in a second-order memristor circuit," in Proceedings of the IEEE International Symposium on Circuits and Systems (ISCAS), 2020.
[37]J. Bisquert and A. Guerrero, "The chemical inductor," J. Am. Chem. Soc. (to be published).
[38]E. M. Izhikevich, *Dynamical Systems in Neuroscience* (MIT Press, 2007).
[39]W. Gerstner, W. M. Kistler, R. Naud, and L. Paninski, *Neuronal Dynamics: From Single Neurons to Networks and Models of Cognition* (Cambridge University Press, 2014).
[40]E. Schöll, *Nonequilibrium Phase Transitions in Semiconductors* (Springer-Verlag, 1987).
[41]M. Keddam, H. Takenouti, and N. Yu, "Transpassive dissolution of Ni in acidic sulfate media: A kinetic model," J. Electrochem. Soc. **132**, 2561–2566 (1985).
[42]E. M. Izhikevich, "Simple model of spiking neurons," IEEE Trans. Neural Networks **14**, 1569–1572 (2003).
[43]C. Rocşoreanu, A. Georgescu, and N. Giurgiţeanu, *The FitzHugh-Nagumo Model: Bifurcation and Dynamics* (Kluwer Academic Publishers, 2000).
[44]T. Kostova, R. Ravindran, and M. Schonbek, "Fitzhugh–Nagumo revisited: Types of bifurcations, periodical forcing and stability regions by a Lyapunov functional," Int. J. Bifurcation Chaos **14**, 913–925 (2004).
[45]D. Armbruster, "The (almost) complete dynamics of the Fitzhugh Nagumo equations," Nonlinear Dyn. **2**, 89–102 (1997).
[46]L. Chua, "Memristor, Hodgkin–Huxley, and edge of chaos," Nanotechnology **24**, 383001 (2013).
[47]Y. V. Pershin and M. Di Ventra, "Memory effects in complex materials and nanoscale systems," Adv. Phys. **60**, 145–227 (2011).
[48]M. T. M. Koper and J. H. Sluyters, "Instabilities and oscillations in simple models of electrocatalytic surface reactions," J. Electroanal. Chem. **371**, 149 (1994).
[49]M. T. M. Koper and J. H. Sluyters, "On the mathematical unification of a class of electrochemical oscillators and their design procedures," J. Electroanal. Chem. **352**, 51 (1993).
[50]M. Berruet, J. C. Pérez-Martínez, B. Romero, C. Gonzales, A. M. Al-Mayouf, A. Guerrero, and J. Bisquert, "Physical model for the current-voltage hysteresis and impedance of halide perovskite memristors," ACS Energy Lett. **7**, 1214–1222 (2022).
[51]D. A. Harrington, "Simplifying mechanistic impedances," Electrochim. Acta **338**, 135895 (2020).
[52]A. Sadkowski, "Small signal local analysis of electrocataytical reaction. Pole-zero approach," J. Electroanal. Chem. **465**, 119–128 (1999).
[53]S. Fletcher, "Tables of degenerate electrical networks for use in the equivalent-circuit analysis of electrochemical systems," J. Electrochem. Soc. **141**, 1823–1826 (1994).
[54]L. Chua, V. Sbitnev, and H. Kim, "Neurons are poised near the edge of chaos," Int. J. Bifurcation Chaos **22**, 1250098 (2012).
[55]A. Ascoli, A. S. Demirkol, R. Tetzlaff, S. Slesazeck, T. Mikolajick, and L. O. Chua, "On local activity and edge of chaos in a NaMLab memristor," Front. Neurosci. **15**, 651452 (2021).
[56]I. Z. Kiss, L. N. Pelster, M. Wickramasinghe, and G. S. Yablonsky, "Frequency of negative differential resistance electrochemical oscillators: Theory and experiments," Phys. Chem. Chem. Phys. **11**, 5720–5728 (2009).
[57]M. T. M. Koper, "Oscillations and complex dynamical bifurcations in electrochemical systems," Adv. Chem. Phys. **92**, 161 (1996).
[58]C. Morris and H. Lecar, "Voltage oscillations in the barnacle giant muscle fiber," Biophys. J. **35**, 193–213 (1981).
[59]J. Nagumo, S. Arimoto, and S. Yoshizawa, "An active pulse transmission line simulating nerve axon," Proc. IRE **50**, 2061–2070 (1962).
[60]K. S. Cole, *Membranes, Ions and Impulses: A Chapter of Classical Biophysics* (University of California Press, 1968).
[61]K. S. Cole, "Rectification and inductance in the squid giant axon," J. Gen. Physiol. **25**, 29–51 (1941).
[62]L. Chua, V. Sbitnev, and H. Kim, "Hodgkin–Huxley axon is made of memristors," Int. J. Bifurcation Chaos **22**, 1230011 (2012).

[63]R. FitzHugh, "Impulses and physiological states in theoretical models of nerve membrane," Biophys. J. **1**, 445–466 (1961).
[64]Q. Wang, Q. Lu, G. Chen, Z. feng, and L. Duan, "Bifurcation and synchronization of synaptically coupled FHN models with time delay," Chaos Solitons Fractals **39**, 918–925 (2009).
[65]D. Fan and L. Hong, "Hopf bifurcation analysis in a synaptically coupled FHN neuron model with delays," Commun. Nonlinear Sci. Numer. Simul. **15**, 1873–1886 (2010).
[66]B. Zhen and J. Xu, "Simple zero singularity analysis in a coupled FitzHugh–Nagumo neural system with delay," Neurocomputing **73**, 874–882 (2010).
[67]Y. Song and J. Xu, "Inphase and antiphase synchronization in a delay-coupled system with applications to a delay-coupled FitzHugh–Nagumo system," IEEE Trans. Neural Networks Learn. Syst. **23**, 1659–1670 (2012).
[68]N. Farajzadeh Tehrani and M. Razvan, "Bifurcation structure of two coupled FHN neurons with delay," Math. Biosci. **270**, 41–56 (2015).
[69]M. M. Ibrahim, M. A. Kamran, M. M. N. Mannan, I. H. Jung, and S. Kim, "Lag synchronization of coupled time-delayed FitzHugh–Nagumo neural networks via feedback control," Sci. Rep. **11**, 3884 (2021).
[70]M. Naito, N. Tanaka, and H. Okamoto, "General relationship between complex impedance and linear stability in electrochemical systems," J. Chem. Phys. **111**, 9908–9917 (1999).
[71]M. T. M. Koper, "Stability study and categorization of electrochemical oscillators by impedance spectroscopy," J. Electroanal. Chem. **409**, 175 (1995).
[72]M. T. M. Koper and J. H. Sluyters, "On the mathematical unification of a class of electrochemical oscillators and their design procedures," J. Electroanal. Chem. **352**, 51 (1993).
[73]M. T. M. Koper, "The theory of electrochemical instabilities," Electrochim. Acta **37**, 1771 (1992).
[74]F. Berthier, J.-P. Diard, C. Montella, and B. Le Gorrec, "Study of the forced Ni/1 M H_2SO_4 oscillator," J. Electroanal. Chem **572**, 267 (2004).
[75]Y. Ushakov, A. Akther, P. Borisov, D. Pattnaik, S. Savel'ev, and A. G. Balanov, "Deterministic mechanisms of spiking in diffusive memristors," Chaos Solitons Fractals **149**, 110997 (2021).
[76]See https://youtu.be/rTGfSfKLuDk for a video with animated cartoons to explain the evolution of impedances by the map of characteristic frequencies.